JACS Au
AN OPEN ACCESS JOURNAL OF THE AMERICAN CHEMICAL SOCIETY

pubs.acs.org/jacsau
Article

Nicotinamide Riboside and CD38: Covalent Inhibition and Live-Cell Labeling

Guoyun Kao,[○] Xiao-Nan Zhang,[○] Fariborz Nasertorabi, Benjamin B. Katz, Zeyang Li, Zhefu Dai, Zeyu Zhang, Lei Zhang, Stan G. Louie, Vadim Cherezov, and Yong Zhang*

Cite This: *JACS Au* 2024, 4, 4345−4360
Read Online

ACCESS | Metrics & More | Article Recommendations | Supporting Information

ABSTRACT: Nicotinamide adenine dinucleotide (NAD^+) is required for a myriad of metabolic, signaling, and post-translational events in cells. Its levels in tissues and organs are closely associated with health conditions. The homeostasis of NAD^+ is regulated by biosynthetic pathways and consuming enzymes. As a membrane-bound protein with robust NAD^+ hydrolase activity, cluster of differentiation 38 (CD38) is a major degrader of NAD^+. Deficiency or inhibition of CD38 enhances NAD^+ levels in vivo, resulting in various therapeutic benefits. As a metabolic precursor of NAD^+, nicotinamide mononucleotide can be rapidly hydrolyzed by CD38, whereas nicotinamide riboside (NR) lacks CD38 substrate activity. Given their structural similarities, we explored the inhibition potential of NR. To our surprise, NR exhibits marked inhibitory activity against CD38 by forming a stable ribosyl−ester bond with the glutamate residue 226 at the active site. Inspired by this discovery, we designed and synthesized a clickable NR featuring an azido substitution at the 5′-OH position. This cell-permeable NR analogue enables covalent labeling and imaging of both extracellular and intracellular CD38 in live cells. Our work discovers an unrecognized molecular function of NR and generates a covalent probe for health-related CD38. These findings offer new insights into the role of NR in modulating NAD^+ metabolism and CD38-mediated signaling as well as an innovative tool for in-depth studies of CD38 in physiology and pathophysiology.

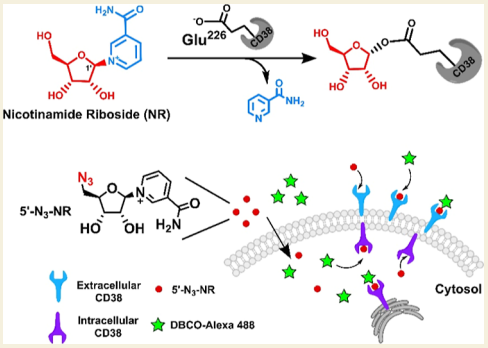

KEYWORDS: *enzymes, nucleosides, inhibitors, CD38, probes*

INTRODUCTION

Nicotinamide adenine dinucleotide (NAD^+) is an essential cofactor participating in a variety of cellular events and processes, such as redox cycling, post-translational modifications, signaling transduction, and epigenetic regulation.[1−7] The decline of NAD^+ levels is associated with aging, neurodegeneration, metabolic diseases, cardiovascular disorders, and other health conditions.[8−14] In addition to de novo and Preiss−Handler pathways, NAD^+ can be synthesized through a salvage pathway from nicotinamide via nicotinamide phosphoribosyltransferase (NAMPT) or from nicotinamide riboside (NR) via NR kinases (NRKs) and nicotinamide mononucleotide (NMN) adenylyltransferases (NMNATs).[15−17] The human genome encodes different classes of enzymes dependent on NAD^+, including oxidoreductases, ADP-ribosyl transferases, ADP-ribosyl cyclases, and sirtuins.[18−23] These degradation enzymes coordinate with those biosynthetic ones to maintain NAD^+ homeostasis, critical for cellular physiology. Dysregulation of the NAD^+ metabolic network tends to contribute to the pathophysiology of many human diseases.[11,24−26]

As a member of the ADP-ribosyl cyclase family, cluster of differentiation 38 (CD38) is a single-pass transmembrane protein, catalyzing the conversion of NAD^+ into cyclic ADP-ribose (cADPR) and ADP-ribose (ADPR) that function as second messengers for endogenous calcium mobilization (Figure 1A).[27−33] The catalytic residue glutamate 226 (E226) at the CD38 active site is involved in the formation of activated intermediates following nicotinamide release, which lead to generation of products (Figure 1A).[34,35] In addition to the cell membrane, CD38 is localized on the membranes of intracellular compartments, such as the endoplasmic reticulum and nucleus. It exists as either a type II or type III membrane protein with an opposite membrane orientation for the C-terminal catalytic domain.[36−39] Like the most common type II CD38, type III CD38 is functionally active in producing the calcium-mobilizing messengers (Figure 1B).[36,37] The membrane-bound CD38 is characterized by robust NAD^+-glycohydrolase (NADase) activity and plays a major role in modulating NAD^+ levels in tissues and organs.[11,13,40−43] Genetic deletion or pharmacological inhib-

Received: August 2, 2024
Revised: October 3, 2024
Accepted: October 21, 2024
Published: October 30, 2024

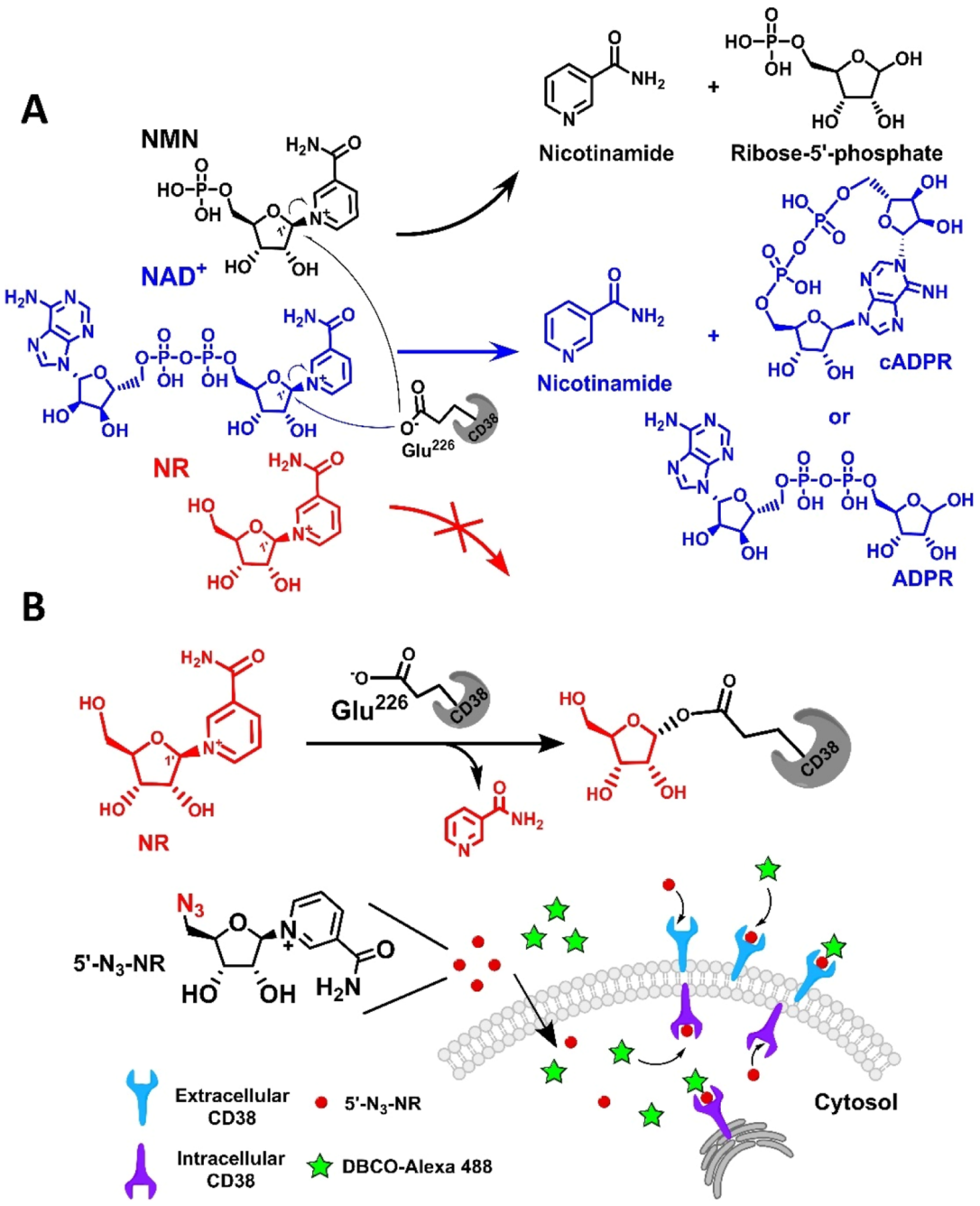

Figure 1. NR and its clickable analogue for covalent inhibition and live-cell labeling of CD38. (A) CD38-catalyzed reactions with NAD^+, NMN, and NR. (B) Covalent inhibition of CD38 by NR and labeling of cellular CD38 by 5′-N_3-NR.

ition of CD38 provides protection from aging-related metabolic disorders, myocardial infarction, nonalcoholic fatty liver disease, neuroinflammation, and fibrosis in preclinical models by augmenting NAD^+ levels in vivo.[9,40,42,44−50]

CD38 is known to hydrolyze NAD^+ and its precursor NMN but lacks enzymatic activity for NR (Figure 1A).[13,51,52] Given the structural similarities between NMN and NR, we asked whether NR could act as an inhibitor of CD38. To our surprise, NR, the metabolic precursor of NAD^+, is found to covalently inhibit CD38 activity by forming a stable ribosyl−ester bond with the E226 residue at the catalytic site (Figure 1B).[53,54] Importantly, our designed clickable NR analogue enables the labeling and imaging of CD38 in living cells (Figure 1B). This work discovers a new functional role of NR and generates a valuable chemical probe for studying CD38 in live-cell conditions.

RESULTS

In addition to the native substrate NAD^+, CD38 recognizes NMN for rapid hydrolysis.[13,52] Compared to the chemical structure of NMN, NR only misses a 5′-phosphate group (Figure 1A) but resists to catalytic cleavage by CD38.[13,51,52] Considering these prior findings, we explored the inhibition potential of NR against CD38. To this end, recombinant CD38 extracellular domain was preincubated in the absence and presence of NMN or NR for 2 h at room temperature (RT). The enzymatic activity of preincubated CD38 was then measured through nicotinamide guanine dinucleotide

https://doi.org/10.1021/jacsau.4c00695
JACS Au 2024, 4, 4345−4360

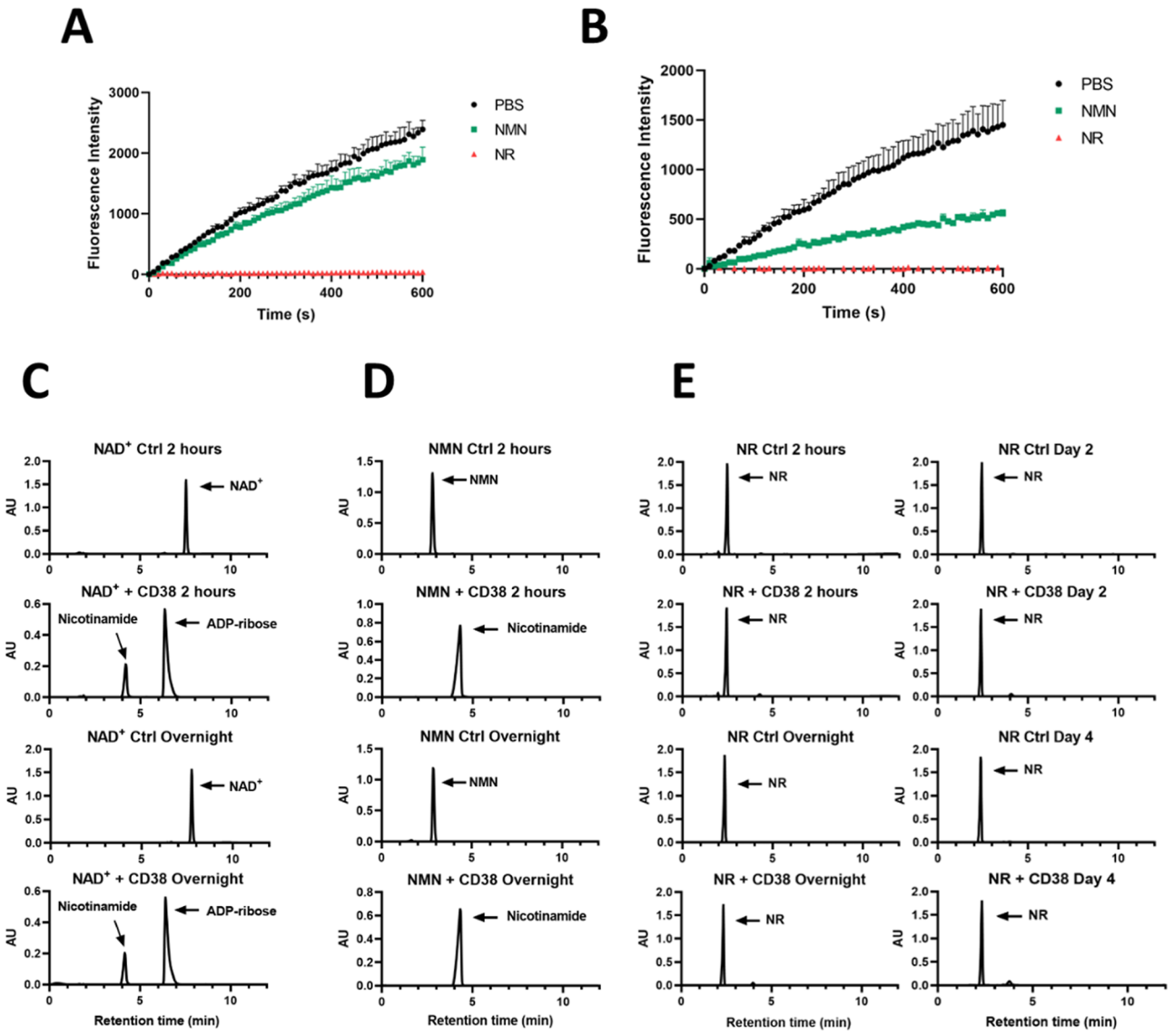

Figure 2. Enzymatic activity of human CD38. (A,B) Monitoring of enzymatic activity of recombinant CD38 extracellular domain via NGD^+-based fluorescence assays after 2 h (A) or overnight (B) incubation in the absence and presence of NMN or NR. CD38 (20 nM) was preincubated without or with NMN or NR (2 μM) for 2 h at RT or overnight on ice, followed by additions of NGD^+ (100 μM) and measurements of the formation of fluorescent cGDPR at 410 nm. (C–E) High-performance liquid chromatography (HPLC) analysis of the enzymatic activity of recombinant CD38 extracellular domain with NAD^+ (C), NMN (D), and NR (E). CD38 (170 nM) was incubated with NAD^+, NMN, or NR (170 μM) for 2 h, overnight, 2 days, or 4 days, followed by HPLC analysis via UV absorbance at 260 nm. Reactions without CD38 under the same conditions were included as controls.

(NGD^+)-based fluorescence assays, in which NGD^+ is converted by catalytically active CD38 into fluorescent cyclic GDP-ribose (cGDPR).[55] Unexpectedly, CD38 pretreated by NR shows no enzymatic activity, whereas the NMN-treated CD38 displays activity comparable to that of CD38 without preincubation with NMN or NR (Figure 2A). Similar results were observed following overnight incubation of CD38 on ice without or with NMN or NR. In contrast to CD38 incubated overnight in PBS, the enzymatic domain of CD38 preincubated overnight with NR gives rise to no catalytic activity with NGD^+ (Figure 2B). These results suggest that NR or its degradation product by CD38 can function as a potent inhibitor for CD38. Interestingly, overnight incubation with NMN reduces CD38 enzymatic activity (Figure 2B), resulted from the nicotinamide product-derived inhibition (Figure S1).

To examine potential NR cleavage by CD38, a HPLC analysis was carried out. In comparison with NAD^+ and NMN controls that are fully converted by CD38 within 2 h to nicotinamide and ADPR and nicotinamide and ribose-5′-phosphate, respectively (Figures 2C,D and S2), less than 1% of NR was consumed following 2 h incubation with CD38 (Figures 2E and S2, and Table S1). Extended incubation of NR with CD38 results in degradation less than 6% within 48 h and below 9% for 96 h (Figure 2E and Table S1). Together with the above NGD^+-based assay results, these data support that NR itself is a CD38 inhibitor.

Next, the inhibition kinetics of NR against CD38 was examined via the NGD^+-based fluorescence assay using various concentrations of NR (Figure 3A). Fluorescence signals indicate dose- and time-dependent inhibition, suggesting that NR is a covalent inhibitor of CD38. An inactivation rate of

https://doi.org/10.1021/jacsau.4c00695
JACS Au 2024, 4, 4345–4360

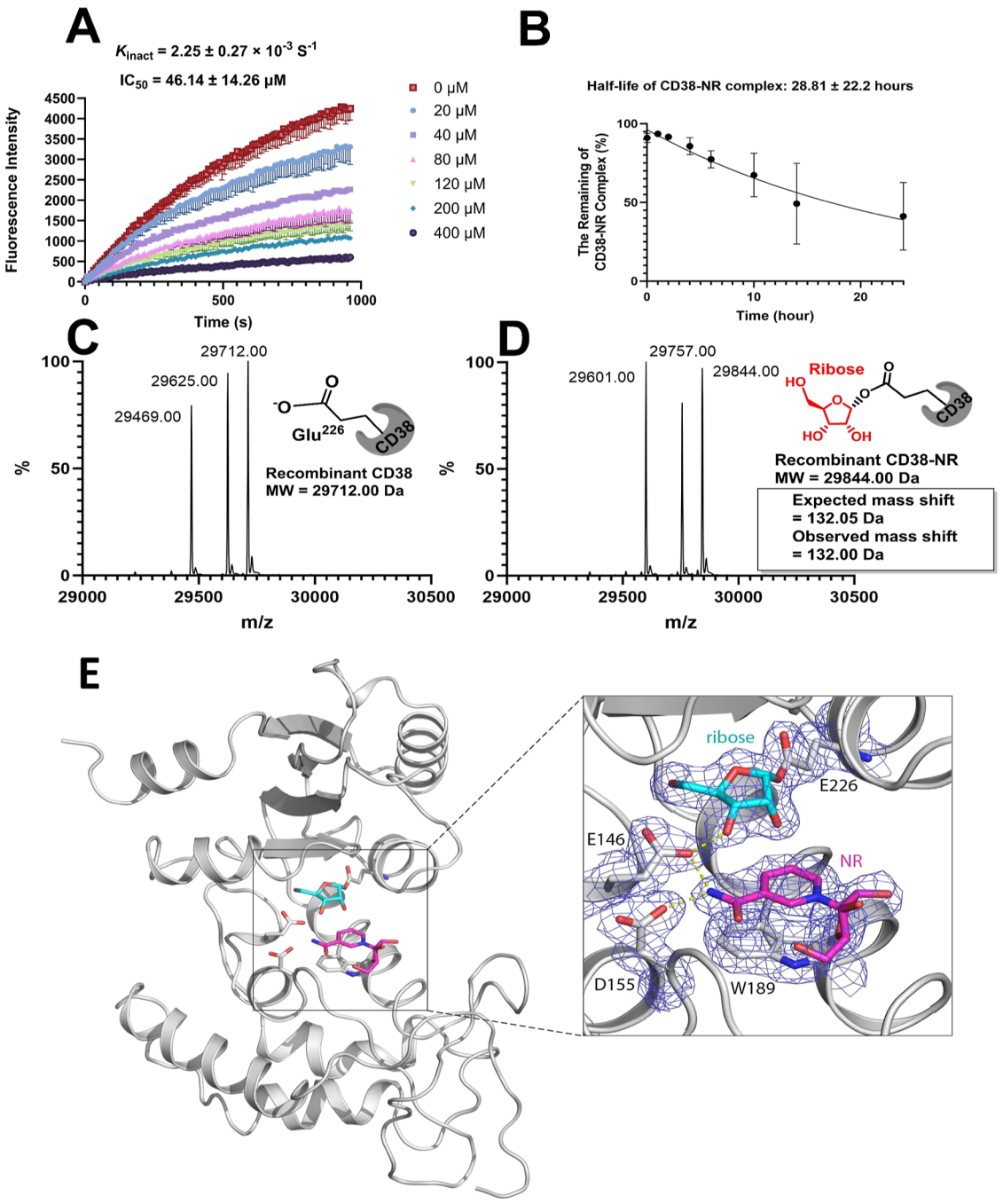

Figure 3. Covalent inhibition of human CD38 by NR. (A) Kinetics of the inactivation of the recombinant CD38 extracellular domain by NR. CD38 was incubated with NGD^+ (100 μM) and varied concentrations of NR in PBS. Its enzymatic activity was monitored based on cGDPR fluorescence at 410 nm. (B) Stability of the CD38-NR complex at a neutral pH. The CD38-NR complex prepared from overnight reactions or CD38 alone was incubated in PBS for 0−24 h, followed by measurements of CD38 catalytic activity via NGD^+-based fluorescence assays to determine the remaining percentages of the CD38-NR complex. (C,D) Mass spectra of the recombinant CD38 extracellular domain (C) and the CD38-NR complex (D). MW, molecular weight. (E) X-ray crystal structure of the human CD38-NR complex. At the zoomed-in active site, the ribose group (cyan) is covalently attached to E226 and the NR ligand (magenta) is stacked against W189 and stabilized by hydrogen bonds with E146 and D155. 2mFo-DFc electron density map is shown as a blue mesh around highlighted residues and ligands at a level of 1 sigma. Hydrogen bonds are shown as yellow dashed lines. PDB ID: 8VAU.

2.25×10^{-3} s^{-1} was determined by fitting the kinetic data into the covalent inhibition equation. Moreover, NGD^+-based fluorescence activity assays revealed that additions of NAD^+, NMN, or nicotinamide at equal molar concentrations result in little changes to the inactivation of CD38 by NR (Figure S3). To evaluate the stability of the potential covalent bond between NR and CD38 at a neutral pH, a complex of CD38-NR was prepared and incubated for up to 24 h to measure the restored CD38 catalytic activity. The half-life of the CD38-NR complex is calculated to be over 28 h (Figures 3B and S4). Furthermore, the presence of nicotinamide reveals no significant changes on the stability of the CD38-NR complex (Figure S5). The CD38-NR complex together with CD38 alone was then analyzed by mass spectrometry. In contrast to

https://doi.org/10.1021/jacsau.4c00695
JACS Au 2024, 4, 4345−4360

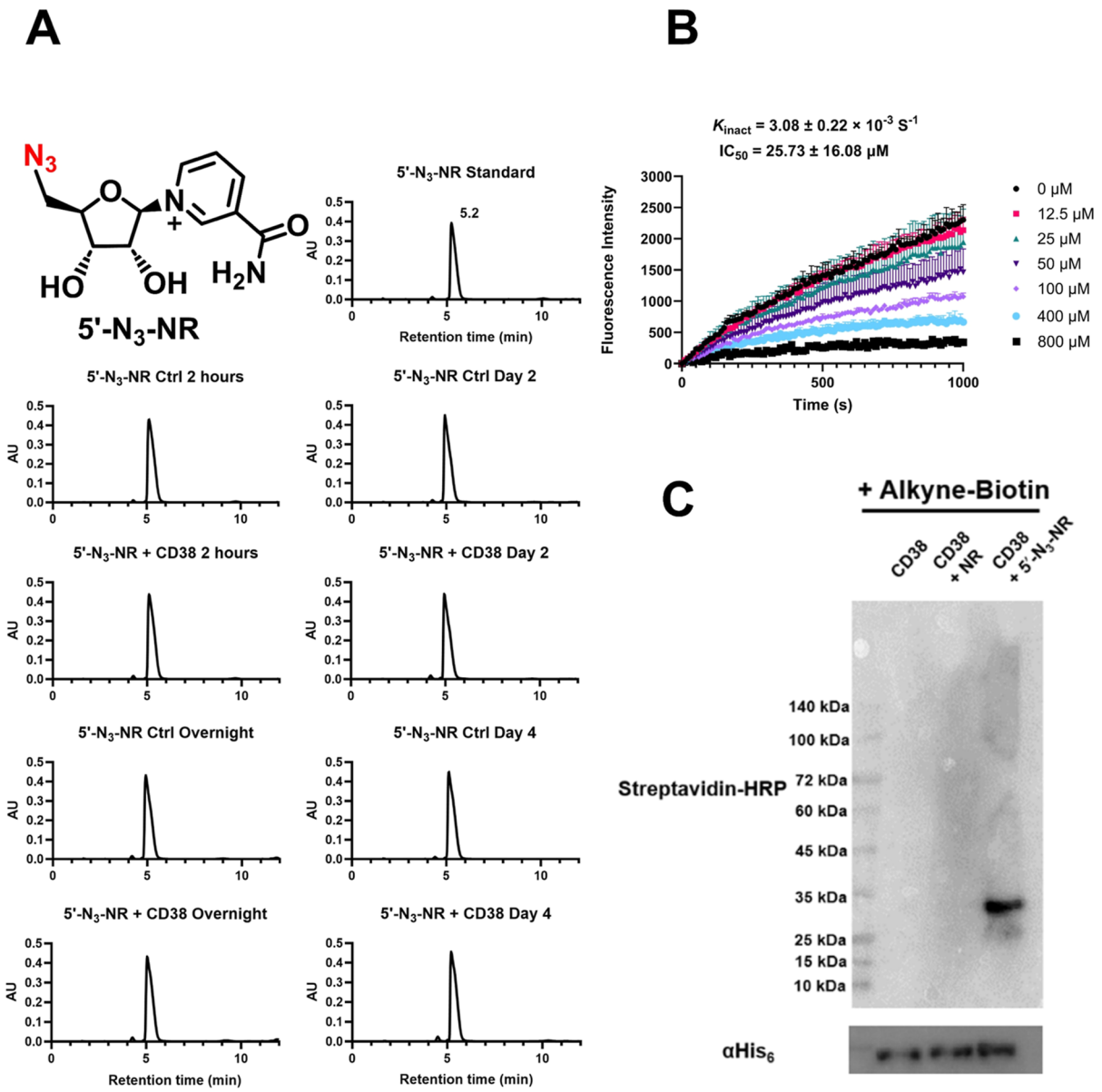

Figure 4. Covalent inhibition of human CD38 by 5′-N_3-NR. (A) Chemical structure of 5′-N_3-NR and HPLC analysis of the enzymatic activity of the recombinant CD38 extracellular domain with 5′-N_3-NR. CD38 (170 nM) was incubated with 5′-N_3-NR (170 μM) for 2 h, 4 days, followed by HPLC analysis via UV absorbance at 260 nm. Reactions without CD38 under the same conditions were included as controls. (B) Kinetics of the inactivation of CD38 by 5′-N_3-NR. The enzymatic activity of CD38 was monitored based on formed fluorescent cGDPR at 410 nm following additions of NGD^+ (100 μM) and various concentrations of 5′-N_3-NR. (C) Immunoblot analysis of labeling of CD38 by 5′-N_3-NR. CD38 was incubated in the absence and presence of NR or 5′-N_3-NR in PBS for 2 h at RT, followed by biotinylation via click chemistry and immunoblots using a streptavidin-HRP conjugate and an anti-His_6 antibody.

the recombinant CD38 extracellular domain, the CD38-NR complex revealed a shift of 132 Da, matching a covalently attached ribose (Figure 3C,D). Mass spectrometric analysis of CD38 and the CD38-NR complex digested by trypsin identified a peptide carrying the ribose group for CD38-NR (Figure S6). Given the presence of catalytic residue E226 within this peptide, we postulate that the NR-derived ribose forms a covalent bond with E226 at the active site. Notably, this covalent attachment was observed in a high-resolution X-ray structure of the CD38-NR complex (Figure 3E and Table S2). At the CD38 catalytic center, a ribose forms a stable ester bond with the side chain of E226 in an α configuration. The resulting nicotinamide from NR cleavage, however, is absent from the binding pocket. Instead, an intact NR ligand with its nicotinamide moiety stacking with the indole ring of W189 and the amide group making hydrogen bonds with side chains of E146 and D155 is found within the active site in addition to the covalently bound ribose. Collectively, these results support the idea that NR can covalently inhibit CD38 and form a stable ribosyl−ester bond with the E226 side chain.

Inspired by the covalent inhibition activity of NR against CD38, we envisioned that a clickable NR analogue could enable the labeling and imaging of CD38 in living cells. To this end, we designed and synthesized 5′-N_3-NR (Figures 4A and S7). Remote from the reaction center, 5′-azido is expected to minimize the effects of chemical modification on the inhibition activity with CD38. Moreover, 5′-azido substitution can block 5′-phosphorylation by NRKs for subsequent metabolic

https://doi.org/10.1021/jacsau.4c00695
JACS Au 2024, 4, 4345−4360

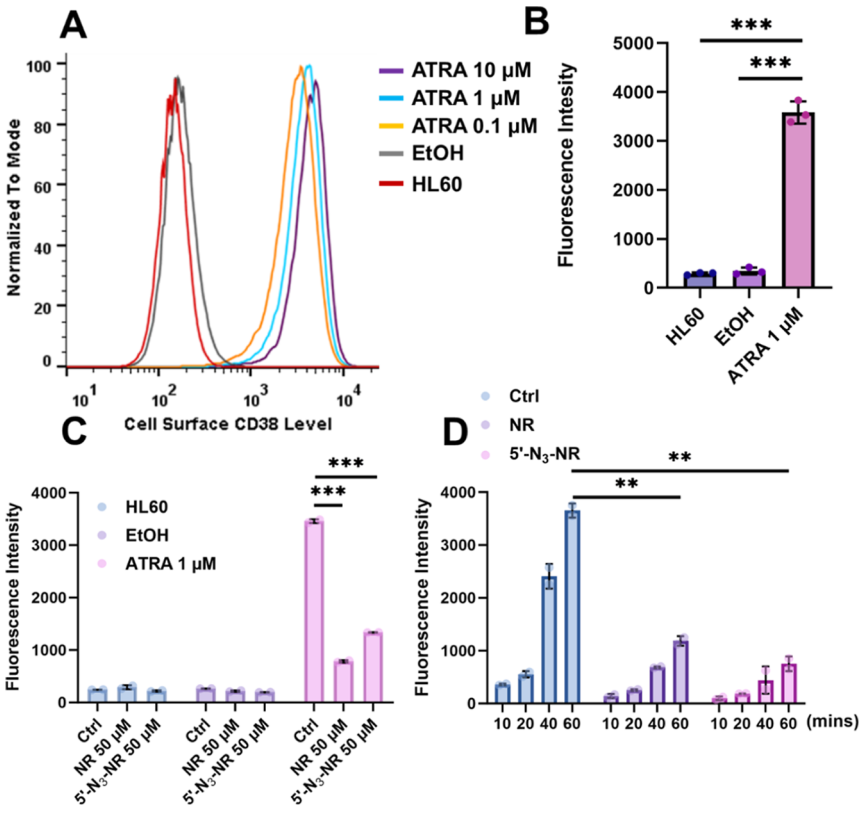

Figure 5. Inhibition of the enzymatic activity of cell-surface CD38 by NR and 5′-N_3-NR. (A) Flow cytometric analysis of CD38 expression levels on HL60 cells after ATRA treatment. HL60 cells were treated without or with ethanol or 0.1−10 μM ATRA for 2 days, followed by flow cytometry. (B) Enzymatic activity of HL60 cell-surface CD38. HL60 cells were treated without or with ethanol or 1 μM ATRA for 2 days. After changing media, cells were incubated with 100 μM NGD^+ for 1 h at 37 °C with 5% CO_2 and centrifuged. The supernatants were measured for cGDPR fluorescence at 410 nm. (C) Inhibition of HL60 cell-surface CD38 activity by NR and 5′-N_3-NR. HL60 cells were treated without or with ethanol or 1 μM ATRA for 2 days and incubated in fresh media without or with 50 μM NR or 5′-N_3-NR for 1 h. After removing media with free NR or 5′-N_3-NR, cells were resuspended in media with 100 μM NGD^+ for 1 h incubation, followed by centrifugation and measurements of cGDPR fluorescence in supernatants. (D) Time course inhibition of cell-surface CD38 by NR and 5′-N_3-NR. HL60 cells treated by 1 μM ATRA for 2 days were incubated with 100 μM NGD^+ for 10−60 min in the absence and presence of 100 μM NR or 5′-N_3-NR, followed by centrifugation and measurements of cGDPR fluorescence in supernatants. $^{**}P < 0.01$ and $^{***}P < 0.001$ by the two-tailed unpaired *t*-test.

conversion, facilitating the stabilization of the cellular levels of 5′-N_3-NR for efficient labeling of CD38.

5′-N_3-NR was first evaluated for substrate activity with CD38 by HPLC. Following up to 4 day incubation with CD38, little degradation of 5′-N_3-NR was observed (Figure 4A and Table S1). The NGD^+-based fluorescence assays indicated that 5′-N_3-NR displays dose- and time-dependent inhibition of CD38 with a k_{inact} of 3.08×10^{-3} s^{-1}, similar to that of NR (Figure 4B). Recombinant CD38 was then incubated in the absence and presence of NR or 5′-N_3-NR for 2 h, followed by additions of alkyne-biotin for click reactions. Immunoblot analysis indicated the successful labeling of CD38 with biotin via 5′-N_3-NR, whereas no biotin signals were detected for CD38 or CD38 with NR (Figure 4C). These results support the idea that 5′-N_3-NR can covalently label CD38 and allow attachments of clickable tags.

Following the discovery of NR and 5′-N_3-NR as covalent inhibitors of recombinant CD38, they were then examined for the inhibitory activity of cellular CD38. The HL60 cell line was chosen as a cellular model as HL60 cells treated with all-trans retinoic acid (ATRA) at 0.1−10 μM for 2 days show significantly increased expression levels of CD38 (Figure 5A). By activating the mitogen-activated protein kinase (MPAK) pathway, ATRA induces the differentiation of HL60 cells and upregulation of CD38 expression.[56,57] ATRA (1 μM) was used for subsequent cellular studies to induce CD38 expression. In comparison to HL60 cells without or with ethanol treatment, ATRA-treated HL60 cells feature substantial CD38 enzymatic activity according to NGD^+-based fluorescence assays (Figure 5B), consistent with CD38 expression levels analyzed by flow cytometry (Figure 5A). Using the same fluorescence assay, the inhibition of NR and 5′-N_3-NR against cell-surface CD38 was evaluated. ATRA-treated HL60 cells that were preincubated with 50 and 100 μM NR or 5′-N_3-NR are characterized by significantly decreased fluorescence intensities in the NGD^+ activity assays relative to those of cells without NR or 5′-N_3-NR (Figure S8). To confirm the covalent inhibition by NR or 5′-N_3-NR, ATRA-treated HL60 cells were washed to remove free compounds following 1 h preincubation with 50 μM NR or 5′-N_3-NR. Subsequent NGD^+ fluorescence assays indicate that the catalytic activity of cell-surface CD38 was markedly inhibited by NR or 5′-N_3-NR (Figure 5C). HL60 cells treated without or with ethanol were included as controls. Furthermore, ATRA-treated HL60 cells were incubated with 100 μM NGD^+ in the absence and presence of 100 μM NR or 5′-N_3-NR. Fluorescence signals for cGDPR were measured for 10−60 min. NR or 5′-N_3-NR exhibits significant inhibition for cellular CD38 catalytic activity (Figure 5D). These results indicate that

https://doi.org/10.1021/jacsau.4c00695
JACS Au 2024, 4, 4345−4360

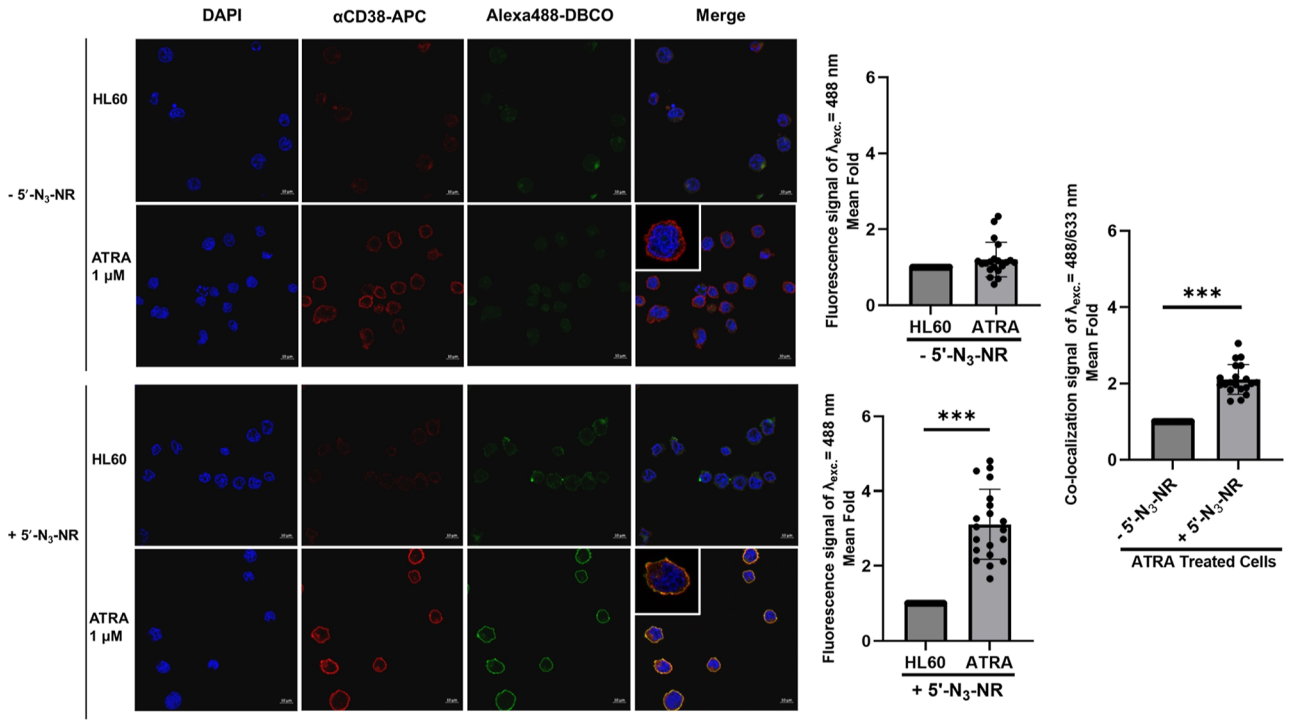

Figure 6. Visualization of cellular CD38 by 5′-N_3-NR. HL60 cells treated without or with 1 μM ATRA for 2 days were incubated in the absence and presence of 100 μM 5′-N_3-NR for 1 h at 37 °C. Cells were then incubated with 10 μM Alexa488-DBCO for 2 h at RT, followed by washing with DPBS, fixation, permeabilization for DAPI as well as anti-CD38-APC staining at RT, and confocal imaging. Scale bars: 10 μm. ***$P < 0.001$ by the two-tailed unpaired *t*-test.

both NR and 5′-N_3-NR can inhibit cell-surface-expressed CD38 activity.

The capability of 5′-N_3-NR to label and visualize cellular CD38 was next studied. HL60 and HL60 treated with ethanol or ATRA were incubated for 1 h in the absence and presence of 100 μM 5′-N_3-NR. Following copper-free click reactions with Alexa488-dibenzocyclooctyne (DBCO), confocal microscopy revealed high levels of 5′-N_3-NR-dependent green fluorescence signals only on surfaces of ATRA-treated HL60 cells, which are suppressed by excess amounts of NR (Figure S9). To further validate the labeling specificity of 5′-N_3-NR, HL60 cells without or with ATRA treatment were stained with an anti-CD38 monoclonal antibody-allophycocyanin (APC) in addition to incubation without and with 5′-N_3-NR and Alexa488-DBCO. Confocal imaging analysis showed upregulated cell-surface CD38 for ATRA-treated cells as detected by the anti-CD38 antibody-APC, which were colocalized with ones labeled by 5′-N_3-NR and Alexa488-DBCO (Figure 6). These results demonstrate that 5′-N_3-NR is a covalent probe for labeling CD38 in live cells.

Since NR is a cell-permeable nucleoside,[15,58] 5′-N_3-NR is likely to efficiently cross cell membrane given their structural similarities, which could enable the labeling of not only cell-surface CD38 but also intracellular CD38 (e.g., type III CD38). After incubating 5′-N_3-NR with HL60 cells for 0−4 h, liquid chromatography−mass spectrometry (LC−MS) quantitative analysis of collected cell pellets and medium indicated rapid cellular uptake and adequate stability in culture medium for 5′-N_3-NR (Figure 7), supporting its potential to covalently label intracellular CD38.

5′-N_3-NR was next applied to label and image upregulated CD38 in live cells. To specifically label intracellular CD38, 2′-F-arabinose NAD^+ (2′-F-araNAD$^+$), a covalent inhibitor of

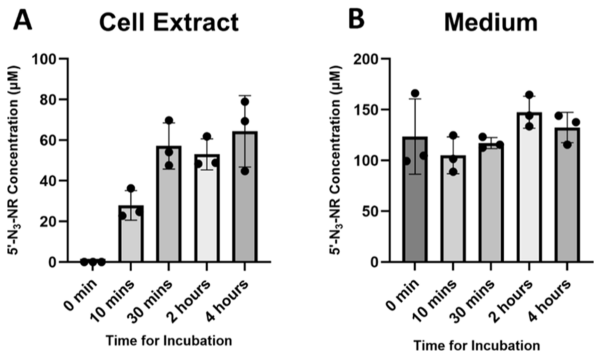

Figure 7. Cellular uptake of 5′-N_3-NR. HL60 cells were incubated with 100 μM 5′-N_3-NR for 0−4 h at 37 °C. After centrifugation, supernatants and cell pellets washed with PBS were collected for quantification of 5′-N_3-NR by LC−MS.

CD38, was synthesized according to previous studies.[28,29,53] Due to low cell permeability, 2′-F-araNAD$^+$ can rapidly label cell-surface CD38, preventing 5′-N_3-NR from targeting extracellular CD38. In addition, a clickable 6-N_3-2′-F-araNAD$^+$ was synthesized (Figure S10), which is expected to allow selective attachment to extracellular CD38 and subsequent fluorescent labeling via click chemistry. Kinetic studies of recombinant CD38 with NGD^+ at various concentrations of 2′-F-araNAD$^+$ and 6-N_3-2′-F-araNAD$^+$ confirm their covalent inhibition activities with k_{inact} of 2.36×10^{-2} s^{-1} for 2′-F-araNAD$^+$ and 1.22×10^{-2} s^{-1} for 6-N_3-2′-F-araNAD$^+$ (Figures S11 and S12).

Upregulation of CD38 expression in HL60 cells was induced by ATRA treatment for 2 or 4 days. Cells without and with ATRA treatment were then incubated with 5′-N_3-NR to covalently label global CD38. To exclusively label extracellular

https://doi.org/10.1021/jacsau.4c00695
JACS Au 2024, 4, 4345−4360

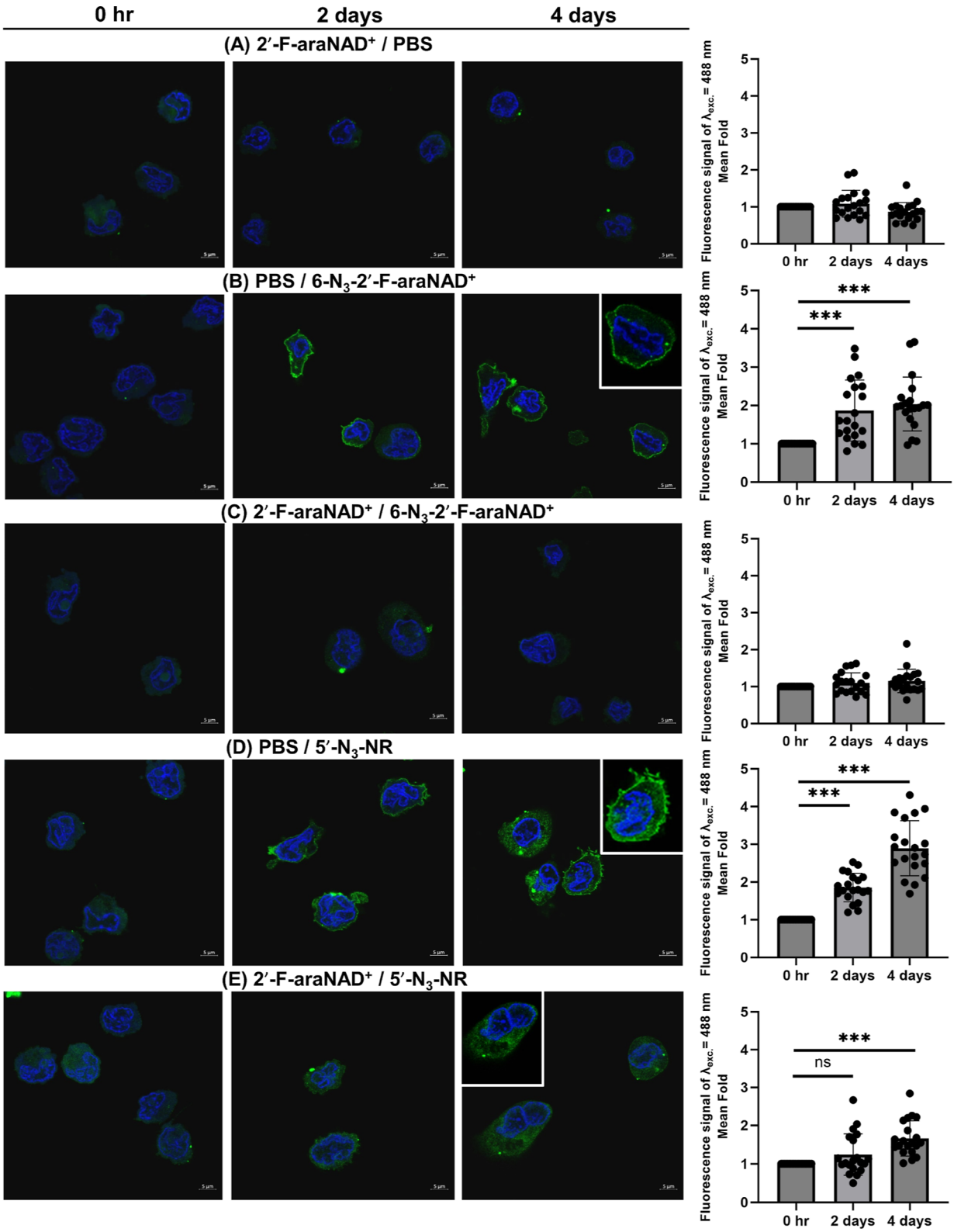

Figure 8. Live-cell imaging of extracellular and intracellular CD38. HL60 cells treated with ATRA for 0, 2, and 4 days were incubated with 100 μM 6-N_3-2′-F-araNAD$^+$ or 5′-N_3-NR to covalently label extracellular CD38 or global CD38, respectively, for 1 h. To block imaging of extracellular CD38, cells were pretreated with 100 μM 2′-F-araNAD$^+$ for 30 min and subsequently incubated without or with 100 μM 6-N_3-2′-F-araNAD$^+$ or 5′-N_3-NR for 1 h. Cells were then incubated with 10 μM Alexa488-DBCO for 2 h at RT, followed by washing with DPBS, fixation, permeabilization for DAPI at RT, and confocal imaging. Scale bars: 5 μm. ns: not significant, $P > 0.05$ and ***$P < 0.001$ by the two-tailed unpaired t-test.

CD38, cells were treated with 6-N_3-2′-F-araNAD$^+$. Following pretreatment with 2′-F-araNAD$^+$, cells were incubated with 5′-N_3-NR for specific attachment to intracellular CD38. Cells treated with 2′-F-araNAD$^+$ only and cells subject to 2′-F-araNAD$^+$ and subsequent 6-N_3-2′-F-araNAD$^+$ treatment were included as controls. CD38 labeled by analogues of NR or

https://doi.org/10.1021/jacsau.4c00695
JACS Au 2024, 4, 4345−4360

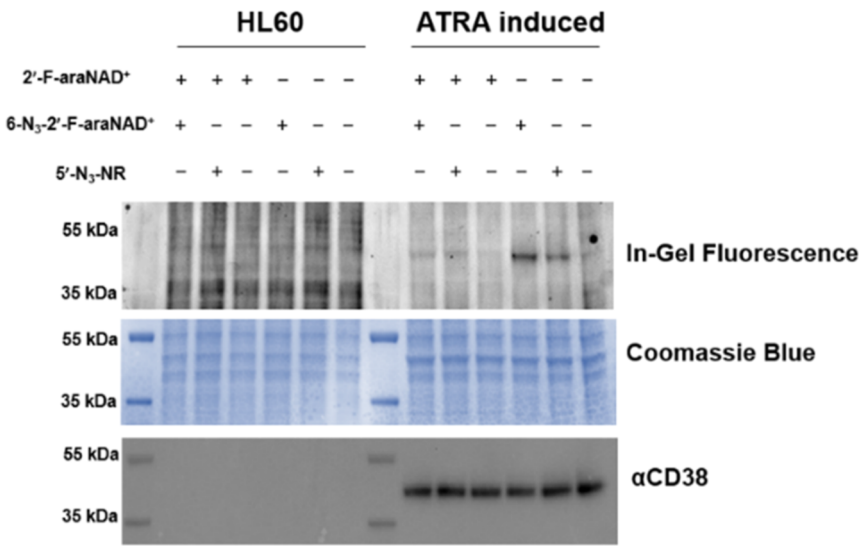

Figure 9. Live-cell labeling of cellular CD38. HL60 cells without or with 4 day treatment by ATRA were incubated with 100 μM 6-N_3-2′-F-araNAD$^+$ or 5′-N_3-NR to covalently label extracellular CD38 or global CD38, respectively, for 1 h. To block the labeling of extracellular CD38, cells were pretreated with 100 μM 2′-F-araNAD$^+$ for 30 min and then incubated without or with 100 μM 6-N_3-2′-F-araNAD$^+$ or 5′-N_3-NR for 1 h. Cells without treatment by 2′-F-araNAD$^+$, 6-N_3-2′-F-araNAD$^+$, or 5′-N_3-NR were included as controls. Following 2 h incubation with 10 μM Alexa488-DBCO, cells were washed with DPBS and lysed. Cell lysates were analyzed by in-gel fluorescence, Coomassie blue staining, and immunoblot using an anti-human CD38 antibody.

NAD$^+$ in live cells was then tagged with Alexa488-DBCO via copper-free click chemistry. It is noted that none of the analogues of NR and NAD$^+$ show significant cytotoxicity for HL60 cells at concentrations up to 250 μM (Figure S13). Confocal imaging analysis indicated significantly enhanced expression of extracellular and global CD38 as stained by 6-N_3-2′-F-araNAD$^+$ and 5′-N_3-NR, respectively, after 2- and 4 day ATRA induction (Figure 8). Notably, extended ATRA treatment of HL60 cells results in considerably increased levels of intracellular CD38 as imaged by 5′-N_3-NR coupled with 2′-F-araNAD$^+$ pretreatment (Figure 8). Due to the lack of azido groups for fluorescent labeling or covalent labeling of extracellular CD38 by the nonclickable NAD$^+$ analogue, no significant Alex488 signals were detected for cells treated by 2′-F-araNAD$^+$ alone or by 2′-F-araNAD$^+$ followed with 6-N_3-2′-F-araNAD$^+$. These findings reveal the time-dependent upregulation of intracellular CD38 in HL60 cells after ATRA treatment.

Labeling of cellular CD38 by 5′-N_3-NR was also examined through in-gel fluorescence. HL60 cells were first cultured for 4 days in the absence or presence of ATRA and then preincubated without or with 2′-F-araNAD$^+$ prior to additions of 5′-N_3-NR or 6-N_3-2′-F-araNAD$^+$. Groups without compound treatment or with 2′-F-araNAD$^+$ alone were included as controls. After copper-free click reactions with Alexa488-DBCO, cells were lysed for SDS-PAGE gel analysis. In-gel fluorescence imaging clearly showed fluorescently labeled CD38 by 5′-N_3-NR or 6-N_3-2′-F-araNAD$^+$ (Figure 9), with lower signal levels for 5′-N_3-NR-treated cells relative to ones by 6-N_3-2′-F-araNAD$^+$. No significant in-gel fluorescent signals were observed for intracellular CD38 as labeled by 5′-N_3-NR after 2′-F-araNAD$^+$ pretreatment. Together with the above confocal images, these results demonstrate 5′-N_3-NR as a covalent probe for studying cellular CD38.

DISCUSSION

NR is a metabolic precursor of NMN and NAD$^+$. Prior studies indicated that nutritional supplementation of NR boosts cellular NAD$^+$ levels through NAD$^+$ biosynthetic pathways.[59−63] In this study, we discover that NR can function as a covalent inhibitor of CD38. The resulting ribosyl−ester bond within the CD38 active site exhibits adequate stability at a neutral pH with a half-life over 28 h. Given the robust NADase activity of membrane-bound CD38 and its major role in the degradation of NAD$^+$, it is likely that supplemented NR not only promotes biosynthesis of NAD$^+$ but also blocks partial consumption of NAD$^+$, a dual mechanism to enhance cellular NAD$^+$ levels. NR in cells and tissues could be converted to NMN by NRKs or degraded by CD157.[51,52] Our work reveals a new physiological role of NR related to CD38 and suggests that in addition to augmenting NAD$^+$ levels, high concentrations of NR can possibly sustain the inhibition of CD38 enzymatic activity, making an impact on calcium signaling through reducing CD38-catalyzed synthesis of second messengers such as cADPR and ADPR. Future studies using appropriate cellular and animal models are needed to test this notion as well as the effects of NR at physiological levels on CD38-modulated signaling activities.

In contrast to NMN that can be rapidly hydrolyzed by CD38, NR only misses 5′-phosphate but lacks efficient conversion into catalytic products. This suggests an important role for the 5′-phosphate in promoting CD38 catalysis. Unlike NAD$^+$ and NMN analogues requiring 2′-F substitutions for the formation of a stable ester bond with the E226 residue,[28,29,53] native NR is shown to be able to react with the E226 side chain, producing a covalent adduct with great stability. It is likely that during and after the reaction with NR, CD38 adopts a conformation different from those with NMN and NAD$^+$, which can protect the generated ribosyl−ester bond from rapid hydrolysis.

As a clickable analogue of NR, 5′-N_3-NR can also covalently inhibit CD38, enabling the labeling of CD38 with fluorescent

https://doi.org/10.1021/jacsau.4c00695
JACS Au 2024, 4, 4345−4360

dyes via click chemistry. Like NR, 5′-N_3-NR is cell permeable but lacks a 5′-OH group for participating in the NAD^+ salvage pathway catalyzed by NRKs and NMNATs. 5′-N_3-NR therefore facilitates the labeling and imaging of intracellular CD38 in live cells. As shown in confocal microscopic studies (Figure 8), expression levels and patterns of intracellular CD38 could undergo dynamic changes. 5′-N_3-NR allows the tracking of intracellular CD38 in a spatiotemporal manner, expanding our biology knowledge of intracellular CD38. In comparison with a 2′-F-araNMN-based, cell-permeable fluorescent probe for CD38,[29] 5′-N_3-NR is likely to possess improved membrane permeability, considering its smaller size and decreased negative charge. This may increase its efficiency for labeling intracellular CD38. Additionally, the clickable azido group of 5′-N_3-NR makes it versatile for attaching different types of tags of interest.

Unlike 6-N_3-2′-F-araNAD$^+$ that can only label extracellular CD38 due to low membrane permeability, 5′-N_3-NR is capable of covalently targeting both extracellular and intracellular CD38. This suggests that CD38 labeled by 5′-N_3-NR would give rise to comparable or higher levels of fluorescence signals than those of CD38 by 6-N_3-2′-F-araNAD$^+$. In-gel fluorescence analysis indicated slightly weaker signals for 5′-N_3-NR-treated cells relative to those of cells incubated with 6-N_3-2′-F-araNAD$^+$. While confocal imaging analysis revealed significant signals for intracellular CD38 through 5′-N_3-NR combined with 2′-F-araNAD$^+$ preincubation, in-gel fluorescence studies showed little CD38 signal for cells with this compound combination. Such lower-than-expected in-gel fluorescence for 5′-N_3-NR-labeled cells could result from reduced accessibility to Alexa488-DBCO and increased sensitivity to proteolytic cleavage after cell lysis.

In summary, this work unveils NR as a covalent inhibitor against CD38, shedding light on its new physiological role in modulating the CD38-mediated NAD^+ metabolism and signaling pathways. The designed 5-N_3-NR permits the labeling of cellular CD38 in live cells, providing a chemical tool to study CD38 in physiological and pathophysiological processes.

MATERIALS AND METHODS

Cell Line

The human leukemia cell line HL60 was purchased from the American Type Culture Collection (VA, USA).

Chemical Synthesis

The details for synthesizing 5′-N_3-NR, 2′-F-araNAD$^+$, and 6-N_3-2′-F-araNAD$^+$ are included in the Supporting Information.[29,54,64,65]

Mammalian Cell Expression and Purification of Recombinant CD38 Extracellular Domain

The DNA plasmid encoding the extracellular domain of human CD38 (R45-I300) was constructed in a previous study.[1] Recombinant CD38 was expressed with the Expi293 expression system (Thermo Fisher Scientific, MA) through transient transfection. Culture media from Expi293F cells, containing the secreted recombinant human CD38, were collected 5 days after transfection. The expressed human CD38 was purified by Ni-NTA chromatography (Thermo Fisher Scientific, MA), followed by washing with wash buffer (20 mM Tris−HCl, pH 8.0, 200 mM NaCl, 30 mM imidazole). The protein was collected with an elution buffer (20 mM Tris−HCl, pH 8.0, 200 mM NaCl, 400 mM imidazole) and further dialyzed in a storage buffer (20 mM Tris−HCl, pH 8.0, 300 mM NaCl). Purified CD38 was concentrated using Amicon centrifugal concentrators (EMD Millipore, Temecula, CA) with a 10 kDa molecular weight cutoff. For crystallization, protein was treated with TEV protease (Thermo Fisher Scientific, MA) to remove the N-terminal poly histidine tag and then purified by following the previous study.[1]

Enzymatic Activities of Recombinant CD38 Protein with NMN and NR

NMN or NR (2 μM, Sigma-Aldrich, MO) was incubated with 20 nM of recombinant CD38 in PBS buffer (pH 7.4) for 2 h at RT or overnight on ice. NGD^+ (100 μM, Sigma-Aldrich, MO) was then added into assay wells, followed by measuring cGDPR levels via fluorescence at 410 nm (excitation at 300 nm) for 10 min at RT by a Synergy H1 plate reader (BioTek, VT).

Inhibition Activities of Nicotinamide and Ribose-5′-Phosphate

Recombinant CD38 (20 nM) in PBS buffer (pH 7.4) without and with overnight incubation on ice in the absence and presence of 2 μM nicotinamide (Sigma-Aldrich, MO), ribose-5′-phosphate (Sigma-Aldrich, MO), or a combination of nicotinamide and ribose-5′-phosphate (molar ratio: 1:1) was measured for enzymatic activities by adding NGD^+ (100 μM) and monitoring subsequently formed cGDPR via fluorescence at 410 nm (excitation at 300 nm) for 10 min at RT using a Synergy H1 plate reader.

HPLC Analysis of Human CD38-Catalyzed Reactions with NAD^+, NMN, NR, or 5′-N_3-NR

NAD^+ (170 μM, Sigma-Aldrich, MO), NMN (170 μM), NR (170 μM), or 5′-N_3-NR (170 μM) was incubated with or without 170 nM recombinant CD38 in PBS buffer (pH 7.4) for 2 h at RT or overnight on ice for NAD^+ and NMN or for 2 h at RT, overnight, 2 days, or 4 days on ice for NR and 5′-N_3-NR. The reaction mixtures underwent analysis by reverse-phase HPLC using a semipreparative C18 Kinetex column (5 μm, 100 Å, 150 × 4.6 mm, from Phenomenex Inc., Torrance, CA) [mobile phase A: 0.1% formic acid (FA) in water; mobile phase B: 0.1% FA in acetonitrile; flow rate = 1.0 mL min^{-1}; 0−10 min: 0−5% B, 10−12 min: 5−0% B] with UV absorbance detection at 260 nm.

Inhibition Activities of NR, 5′-N_3-NR, 2′-F-araNAD$^+$, and 6-N_3-2′-F-araNAD$^+$ for CD38

NR, 5′-N_3-NR, 2′-F-araNAD$^+$, or 6-N_3-2′-F-araNAD$^+$ at various concentrations was incubated with 20−100 nM recombinant CD38 and 100 μM NGD^+ in PBS buffer (pH 7.4). Reactions were monitored at RT via fluorescence at 410 nm (excitation at 300 nm) for 800−1000 s by a Synergy H1 plate reader. The initial reaction velocities ($v_{initial}$) in the presence of different concentrations of compounds were used to determine the inactivation constant (k_{inact}) as follows: $[P] = v_{initial}(1 - \exp(-k_{obs}t))/k_{obs}$ and $k_{obs} = k_{inact}[I]/([I] + K_i)$. [P] is the level of product generated at different time points; $v_{initial}$ is the initial reaction rate; k_{obs} is the rate constant; k_{inact} is the inactivation rate constant for the covalent inhibitor; [I] is the concentration of covalent inhibitor; and K_i is the concentration of covalent inhibitor approaching an inactivation rate equal to half of k_{inact}. The equation was entered into GraphPad Prism (GraphPad Software, CA) to calculate k_{inact}. Reaction velocities at various compound concentrations were used to determine the IC_{50} via GraphPad Prism.

Effects of NAD^+, NMN, and Nicotinamide on the Inhibition of CD38 by NR

Recombinant CD38 (20 nM) in PBS buffer (pH 7.4) in the absence and presence of 100 μM NR mixed without and with 100 μM NAD^+, NMN, or nicotinamide was measured for enzymatic activities through additions of 100 μM NGD^+. Reactions were monitored at RT via fluorescence at 410 nm (excitation at 300 nm) using a Synergy H1 plate reader.

Stability of the CD38-NR Covalent Complex

NR (500 μM) was incubated with 5 μM CD38 in PBS buffer (pH 7.4) overnight on ice. The CD38-NR covalent complex was purified and concentrated using 10 kDa molecular weight cutoff Amicon centrifugal concentrators (EMD Millipore, Temecula, CA). The

https://doi.org/10.1021/jacsau.4c00695
JACS Au 2024, 4, 4345−4360

concentration of the protein complex was determined using a NanoDrop 2000C spectrophotometer (Thermo Fisher Scientific, Waltham, MA). Recombinant CD38 or CD38-NR complex (50 nM) was then incubated in PBS buffer (pH 7.4) at RT for 0, 1, 2, 4, 6, 10, 14, and 24 h. After incubation, 100 μM NGD^+ was added into each sample, followed by measuring the fluorescence intensity at 410 nm (excitation at 300 nm) for 10 min at RT by a Synergy H1 plate reader. The initial velocities of the NGD^+ reactions for samples from different incubation time points were measured to calculate the remaining percentages of the CD38-NR complex as follows: CD38-NR (%) = 100% × (1 − (velocity of cGDPR formation from CD38-NR)/(velocity of cGDPR formation from recombinant CD38)).

To determine the stability of the CD38-NR complex in the presence of nicotinamide, recombinant CD38 or CD38-NR complex (60 nM) was incubated in PBS in the absence or presence of nicotinamide at a molar ratio of 1:100 or 1:200 at RT for 0, 2, 6, and 12 h, followed by measurements of CD38 catalytic activity via NGD^+-based fluorescence assays as described above.

Mass Spectrometry of the CD38-NR Covalent Complex

All protein samples were diluted to 0.2 mg mL^{-1} in 50 mM ammonium bicarbonate (pH 8.0). Glycans were removed using 1:100 (w/w) PNGaseF (New England Biolabs, MA) at 37 °C overnight. The intermolecular disulfide bonds were cleaved using 0.1 M dithiothreitol for 5 min at RT. Samples (4 μL) were injected into an LC−MS instrument using the method below.

Intact protein samples were analyzed by LC−MS [ACQUITY ultraperformance liquid chromatography (UPLC) H-class system, Xevo G2-XS QTOF, Waters Corporation]. Proteins were separated away from reaction buffer salts using a phenyl guard column (ACQUITY UPLC BEH Phenyl VanGuard precolumn, 130 Å, 1.7 μm, 2.1 mm × 5 mm, Waters Corporation). The 5 min method used a flow rate of 0.2 mL min^{-1} with a gradient of buffer A consisting of 0.1% FA in water (water LC−MS #9831-02, JT Baker; FA LC−MS #85178, Thermo Fisher Scientific) and buffer B, acetonitrile (acetonitrile UHPLC/MS #A956, Thermo Fisher Scientific). The gradient running program (flow rate set at 0.2 mL min^{-1} and curve set as 6) is as follows: maintaining 100% buffer A from 0 to 30 s, adjusting to 10% buffer A and 90% buffer B from 30 to 120 s as a gradient, maintaining 10% buffer A and 90% buffer B from 120 to 150 s, reaching to 100% buffer A from 150 to 240 s as a gradient, and maintaining 100% buffer A from 240 to 300 s.

The Xevo Z-spray source was operated in positive MS resolution mode with a capillary voltage of 3000 V and a cone voltage of 40 V (NaCsI calibration, Leu-enkephalin lock-mass). Nitrogen was used as the desolvation gas with a total flow of 800 L h^{-1}. Total average mass spectra were reconstructed from the charge state ion series using the MaxEnt1 algorithm from Waters MassLynx software V4.1 SCN949 according to the manufacturer's instructions. To obtain the ion series described, the major peaks of the chromatogram were selected for integration before further analysis.

Mass Spectrometry of the Conjugation Site of the CD38-NR Complex

Recombinant CD38 and CD38-NR complexes were subjected to overnight solution digestion with trypsin gold (Promega) at 37 °C and pH 8.5. All LC−MS/MS experiments were performed using the same Waters Xevo QTOF setup and buffer system as the intact protein analysis described above. Separation of peptides was performed by reversed-phase chromatography using a reversed-phase C4 column (ACQUITY UPLC Protein BEH C4 Column, 300 Å, 1.7 μm, 2.1 mm × 50 mm, Waters Corporation). The gradient running program (flow rate set at 0.3 mL min^{-1} and curve set as 6) is as follows: maintaining 97% buffer A and 3% buffer B from 0 to 30 s, reaching to 40% buffer A and 60% buffer B from 30 to 120 s as a gradient, maintaining 40% buffer A and 60% buffer B from 120 to 150 s, reaching to 10% buffer A and 90% buffer B from 150 to 180 s as a gradient, maintaining 10% buffer A and 90% buffer B from 180 to 210 s, reaching to 97% buffer A and 3% buffer B from 210 to 240 s as a gradient, and maintaining 97% buffer A and 3% buffer B from 240 to 300 s.

Peptide data were acquired after a 0.5 min waste diversion to remove buffer salts. The Xevo Z-spray source was operated with a capillary voltage of 3000 V and a cone voltage of 40 V (NaCsI calibration, Leu-enkephalin lock-mass). Nitrogen was used as the desolvation gas with a total flow of 800 L h^{-1}. Data were acquired across the 100 to 2000 Da range in MSe continuum mode with alternating 0.5 s scans at alternating collision energy, low energy, 0 V, and a high collision energy ramp (15 to 45 V). The high energy data correspond to the MS2 secondary fragmentation of the low energy scans of similar time.

The peptide digest MSe data were processed for exact mass peptide matching and b&y ion fragmentation mapping using BiopharmaLynx software (Version 1.3.5 Waters Corporation). The software generates in-silico peptide digestion data including all potential modifications and maps the deconvolved MSe data at 30 ppm (parts per million) error to the theoretically calculated masses.

X-ray Crystallography of the CD38-NR Complex

Recombinant CD38 was eluted from a Superdex 75 Increase 10/300 GL column (GE Healthcare Life Sciences, Pittsburgh, PA) in 15 mM HEPES (pH 7.5) and 50 mM NaCl and concentrated to 2.2 mg mL^{-1} at 4 °C. Crystallization was performed at 22 °C using the vapor diffusion method in a hanging-drop setup in 24-well VDX plates (Hampton Research) with a 1:1 ratio of 1 μL of reservoir solution and 1 μL of protein solution against 500 μL of reservoir solution. Initial crystals grew under similar conditions as in the previously published work.[1]

The optimized conditions for the crystal growth were 100 mM HEPES (pH 7.0) and 14−16% PEG 3350. The native crystals with an average size of 50 × 100 μm were soaked for an hour in a cryo-solution containing 10 mM NR (100 mM HEPES at pH 7.0, 25% PEG 3350, 8% glycerol, and 10 mM NR). The crystals were carefully flash-frozen in liquid nitrogen before they were mounted for data collection at the synchrotron.

Crystallographic data were collected at the Stanford Synchrotron Radiation Lightsource (SSRL) using beamline 12-1 equipped with an Eiger X 16 M detector (Dectris). The X-ray beam was attenuated by 85%, and diffraction images were collected by using 0.1 s exposure and 0.1° oscillation for a total of 270° of rotation. The collected data were indexed and integrated with X-ray Detector Software and scaled using Scala, a part of the CCP4 suite.[66−68] Initial phase information was obtained by molecular replacement using PHASER with the previously solved structure of the human CD38−4′-thioribose NAD^+ complex (PDB ID: 6EDR) as the search model.[69] Waters were added using ARP/wARP during the initial round of the refinement.[70] The structure was improved by iterative rounds of model building and refinement using the programs Coot and Refmac5.[71,72] The final rounds of refinement were performed using Phenix.refine part of the phenix software package (v. 1.20.1_4487).[73]

The crystals belong to the monoclinic space group $P2_1$ with two molecules per asymmetric unit and the Mathew's coefficient of 2.38. Crystallographic details and statistics are listed in Table S2.

Immunoblot Analysis of Labeling of CD38 by 5′-N_3-NR

Recombinant CD38 (6 μM) was incubated in the absence and presence of 5′-N_3-NR or NR (600 μM) for 2 h at RT. The mixtures were then incubated with alkyne-biotin for copper(I)-catalyzed azide alkyne cycloaddition (CuAAC) for 2 h at RT in a volume of 15 μL, consisting of 10 μL protein mixtures, 0.5 mM THPTA, 0.25 mM $CuSO_4$, 100 μM alkyne-biotin, and 2.5 mM sodium ascorbate in PBS. Subsequently, reactions were analyzed by immunoblots using a streptavidin-HRP conjugate (R&D Systems, Minneapolis, MN; 1:200 dilution) and an anti-His_6 primary antibody (Thermo Fisher Scientific, Waltham, MA; 1:2000 dilution) and goat anti-mouse secondary IgG antibody-HRP conjugate (Thermo Fisher Scientific, Waltham, MA; 1:3000 dilution).

https://doi.org/10.1021/jacsau.4c00695
JACS Au 2024, 4, 4345−4360

Flow Cytometry of CD38 Expression

HL60 cells were cultured in RPMI 1640 medium (Corning, NY) with 10% FBS (Thermo Fisher Scientific, MA) in an incubator with 5% CO_2 at 37 °C. Cells were treated with 0.1, 1, and 10 μM ATRA (Sigma-Aldrich, MO) for 2 days to induce CD38 expression. After ATRA treatment, cells were centrifuged at 200*g* for 5 min. Cell pellets were washed and resuspended in 5 mL of DPBS, followed by centrifugation at 200*g* for 5 min. Cells were resuspended in 500 μL of ice-cold DPBS with 200 nM anti-CD38 IgG conjugated with FITC (BioLegend, San Diego, CA) and incubated at 4 °C for 30 min, followed by DPBS washing and resuspension in 500 μL of ice-cold DPBS for flow cytometric analysis using a BD Fortessa X20 Cell Analyzer (BD Bioscience, CA) for FITC intensities. Cells without ATRA treatment and cells treated with EtOH for 2 days were included as controls.

Enzymatic Activity of Cell-Surface CD38

HL60 cells were first treated with 1 μM ATRA for 2 days to induce CD38 expression and then centrifuged at 200*g* for 5 min to remove media. 1 million cells were incubated in 200 μL of cell media with 100 μM NGD^+ for 1 h in an incubator with 5% CO_2 at 37 °C, followed by centrifugation at 200*g* for 5 min. Collected supernatants (100 μL) were measured for cGDPR formation via fluorescence at 410 nm (excitation at 300 nm) by a Synergy H1 plate reader. Cells without ATRA treatment and cells treated with EtOH for 2 days were included as controls.

Inhibition Activity of NR and 5′-N_3-NR for Cell-Surface CD38

HL60 cells were first treated with 1 μM ATRA for 2 days to induce CD38 expression and then centrifuged at 200*g* for 5 min to remove media. For assays without removals of NR or 5′-N_3-NR, 1 million cells were incubated in 100 μL of cell media with 50 or 100 μM NR or 5′-N_3-NR for 1 h in an incubator with 5% CO_2 at 37 °C, followed by additions of 100 μM NGD^+ for additional 1 h incubation in the same incubator. For assays with NR or 5′-N_3-NR removed before additions of NGD^+, 1 million cells were incubated in 100 μL of cell media with 50 μM NR or 5′-N_3-NR for 1 h in an incubator with 5% CO_2 at 37 °C, followed by centrifugation at 200*g* for 5 min. Cell pellets were washed with DPBS three times and incubated with 100 μM NGD^+ in cell media for 1 h in the same incubator. After incubation with NGD^+, above cells were centrifuged at 200*g* for 5 min and supernatants (100 μL) were measured for cGDPR formation via fluorescence at 410 nm (excitation at 300 nm) by a Synergy H1 plate reader. Cells without ATRA treatment and cells treated with EtOH for 2 days were included as controls.

To evaluate the time course inhibition of cell-surface CD38 by NR and 5′-N_3-NR, 1 million HL60 cells treated with 1 μM ATRA for 2 days were incubated in 200 μL of cell media with 100 μM NGD^+ in the absence and presence 100 μM NR or 5′-N_3-NR for 10, 20, 40, and 60 min in an incubator with 5% CO_2 at 37 °C. At each incubation time point, cells were centrifuged at 200*g* for 5 min and supernatants (100 μL) were measured for cGDPR formation via fluorescence at 410 nm (excitation at 300 nm) by a Synergy H1 plate reader.

Confocal Microscopy of Cellular CD38 by 5′-N_3-NR

HL60 cells were treated without or with ethanol or 1 μM ATRA for 2 days, followed by 1 h incubation in the absence and presence of 100 μM 5′-N_3-NR at 37 °C. Additionally, ATRA-treated HL60 cells were incubated with 100 μM 5′-N_3-NR without and with 500 μM NR for 1 h at 37 °C. Cells were subsequently centrifuged at 200*g* for 5 min and resuspended in fresh media for labeling without or with 10 μM Alexa488-DBCO (Click Chemistry Tools, Scottsdale, AZ) for 2 h at RT. After washing three times with PBS, cells were fixed with 4% paraformaldehyde solution in DPBS (Santa Cruz Biotechnology, Dallas, TX) for 20 min at RT and washed three times with PBS. Subsequently, cells were permeabilized with 0.5% Triton X-100 (Sigma-Aldrich, MO) for 20 min at RT, washed three times with PBS, stained with DAPI (1 μg mL^{-1} in PBS, Sigma-Aldrich, MO) and an anti-human CD38-APC conjugate (BioLegend, San Diego, CA) at RT, and washed three times with PBS. Confocal microscopic analysis was performed using a Zeiss LSM 880 confocal laser scanning microscope (Carl Zeiss Microscopy, White Plains, NY) equipped with a 63×, 1.4 oil immersion objective lens. DAPI, Alexa488, and APC were excited at 405, 488, and 633 nm, respectively. Images were processed using Zeiss Zen Black software (Carl Zeiss Microscopy, White Plains, NY).

Cell Uptake of 5′-N_3-NR

One million HL60 cells were incubated with 100 μM 5′-N_3-NR for 0, 10 min, 30 min, 2 h, and 4 h in RPMI 1640 media with 10% FBS, followed by centrifugation at 200*g* for 5 min to collect cell pellets and supernatants for the quantification of 5′-N_3-NR by liquid chromatography−mass spectrometry (LC−MS). Methanol (100%) with internal standard methotrexate (MTX) in a volume of 400 μL was used for cell extraction at each time point. Media samples (100 μL) at each time point were extracted by 300 μL methanol (100%) with internal standard MTX. Standard curves of 5′-N_3-NR in media and cell extract were prepared by spiking 0.1, 0.5, 1, 5, 10, 50, 100, 500, and 1000 ng mL^{-1} 5′-N_3-NR into blank RPMI 1640 media with 10% FBS or cell extract from 1 million HL60 cells, with internal standard MTX. Protein concentrations for cell extract samples were determined by Bradford assays.

The extracted analytes were centrifuged to remove protein precipitations and subjected to LC−MS. An Ultracore SuperC18 column (ACE, 5 μm, 50 mm × 3 mm, 100 Å) was used for separation. The concentrations of analytes after separation were quantified by a triple-quadrupole tandem mass spectrometer operating in positive mode with electrospray ionization (ESI) mode. 5′-N_3-NR and MTX were detected using multiple-reaction-monitoring (MRM). The running time for each assay was 6 min. Parameters for LC are as follows: mobile phase A, H_2O with 0.1% FA; mobile phase B, methanol with 0.1% FA; flow rate, 0.2 mL min^{-1}; 50% buffer A and 50% buffer B from 0 to 6 min.

Cytotoxicity of NR and Analogues of NR and NAD^+

HL60 cells and ATRA-treated HL60 cells were incubated with 100 or 250 μM NR, 5′-N_3-NR, 2′-F-araNAD$^+$, and 6-N_3-2′-F-araNAD$^+$ for 24 h at 37 °C. Untreated cells were included as controls. Cells were then centrifuged at 200*g* for 5 min and washed and resuspended in 5 mL of DPBS. Following centrifugation at 200*g* for 5 min, cells were resuspended in 100 μL of DPBS with Zombie Aqua fluorescent dye (BioLegend, San Diego, CA), and incubated at RT for 30 min. After washing and resuspending in DPBS, cells were analyzed using a BD Fortessa X20 Cell Analyzer for Brilliant Violet 510 intensities.

Confocal Microscopy of Extracellular and Intracellular CD38

HL60 cells were treated with 1 μM ATRA for 0, 2, and 4 days to induce CD38 expression, followed by incubation with 100 μM 6-N_3-2′-F-araNAD$^+$ or 5′-N_3-NR for 1 h at 37 °C and washing with DPBS. To block the imaging of extracellular CD38, HL60 cells were preincubated with 100 μM 2′-F-araNAD$^+$ for 30 min at 37 °C, followed by 1 h incubation without or with 100 μM 6-N_3-2′-F-araNAD$^+$ or 5′-N_3-NR at 37 °C and subsequent washing with DPBS. Cells were then labeled with 10 μM Alexa488-DBCO through click reactions for 2 h at RT and washed three times with DPBS. After fixation with 4% paraformaldehyde solution in PBS for 20 min at RT, cells were washed three times with PBS, permeabilized with 0.5% Triton X-100 for 20 min at RT, washed with DPBS for three times, stained with DAPI (1 μg mL^{-1} in PBS) at RT, and washed three times with DPBS. An LMS880 confocal laser scanning microscope was used for confocal microscopic analysis. Twenty cells in each group were selected to quantify the fluorescence mean via the FIJI plugin. Fluorescence mean for the group of 0 h treatment with ATRA was set as the baseline and fluorescence mean for the groups of 2 and 4 day treatment with ATRA was divided by the baseline to calculate fluorescence mean fold via GraphPad Prism.

https://doi.org/10.1021/jacsau.4c00695
JACS Au 2024, 4, 4345−4360

Live-Cell Labeling of Cellular CD38

HL60 cells were treated without or with 1 μM ATRA for 4 days to induce CD38 expression, followed by incubation with 100 μM 6-N_3-2′-F-araNAD$^+$ or 5′-N_3-NR for 1 h at 37 °C and washing with DPBS. To block the labeling of extracellular CD38, HL60 cells were preincubated with 100 μM 2′-F-araNAD$^+$ for 30 min at 37 °C, followed by 1 h incubation without or with 100 μM 6-N_3-2′-F-araNAD$^+$ or 5′-N_3-NR at 37 °C and subsequent washing with DPBS. Cells without treatment by 2′-F-araNAD$^+$, 6-N_3-2′-F-araNAD$^+$, or 5′-N_3-NR were included as controls. Cells were then labeled with 10 μM Alexa488-DBCO through click reactions for 2 h at RT and washed three times with DPBS. Cell pellets were resuspended in 200 μL of lysis buffer [25 mM Tris−HCl pH 7.5, 50 mM NaCl, 10% glycerol, 1% Nonidet P-40 (VWR, Radnor, PA), and Halt Protease Inhibitor Cocktail (Sigma-Aldrich, MO)] for 20 min on ice. Protein concentrations of cell lysates were determined with Bradford reagents (Thermo Fisher Scientific, MA). Cell lysates were loaded onto ExpressPlus-PAGE gels (GenScript, Piscataway, NJ) for analysis through in-gel fluorescence and Coomassie blue staining using an iBright Imaging System (Thermo Fisher Scientific, MA) as well as immunoblots using an anti-human CD38 primary antibody (BioLegend, San Diego, CA; 1:2000 dilution) and a secondary goat anti-mouse IgG antibody-HRP conjugate (Thermo Fisher Scientific, Waltham, MA; 1:3000 dilution).

Statistical Analysis

Two-tailed unpaired t tests were used for comparison between the two groups. Significance of finding was defined as follows: ns = not significant; $P > 0.05$; *$P < 0.05$; **$P < 0.01$; and ***$P < 0.001$. Data are shown as mean ± SD (n = 2, 3 or 20). All statistical analyses were calculated with GraphPad Prism.

■ ASSOCIATED CONTENT

Data Availability Statement

The authors confirm that the data supporting the findings of this study are available from the corresponding author upon request. Coordinates and structure factors of the solved X-ray structure of the human CD38 catalytic domain with covalently attached ribose have been deposited in the Protein Data Bank with the PDB ID 8VAU.

Supporting Information

The Supporting Information is available free of charge at https://pubs.acs.org/doi/10.1021/jacsau.4c00695.

Additional results and experimental details of chemical synthesis (PDF)

■ AUTHOR INFORMATION

Corresponding Author

Yong Zhang − *Department of Pharmacology and Pharmaceutical Sciences, Alfred E. Mann School of Pharmacy and Pharmaceutical Sciences, University of Southern California, Los Angeles, California 90089, United States; Department of Chemistry, Dornsife College of Letters, Arts and Sciences, Norris Comprehensive Cancer Center, and Research Center for Liver Diseases, University of Southern California, Los Angeles, California 90089, United States;* orcid.org/0000-0002-3132-8557; Email: yongz@usc.edu

Authors

Guoyun Kao − *Department of Pharmacology and Pharmaceutical Sciences, Alfred E. Mann School of Pharmacy and Pharmaceutical Sciences, University of Southern California, Los Angeles, California 90089, United States*

Xiao-Nan Zhang − *Department of Pharmacology and Pharmaceutical Sciences, Alfred E. Mann School of Pharmacy and Pharmaceutical Sciences, University of Southern California, Los Angeles, California 90089, United States;* orcid.org/0000-0002-9780-6507

Fariborz Nasertorabi − *Departments of Biological Sciences and Chemistry, Bridge Institute, Michelson Center for Convergent Bioscience, USC Structure Biology Center, University of Southern California, Los Angeles, California 90089, United States*

Benjamin B. Katz − *Department of Chemistry, University of California Irvine, Irvine, California 92697, United States*

Zeyang Li − *Titus Family Department of Clinical Pharmacy, Alfred E. Mann School of Pharmacy and Pharmaceutical Sciences, University of Southern California, Los Angeles, California 90089, United States*

Zhefu Dai − *Department of Pharmacology and Pharmaceutical Sciences, Alfred E. Mann School of Pharmacy and Pharmaceutical Sciences, University of Southern California, Los Angeles, California 90089, United States*

Zeyu Zhang − *Department of Pharmacology and Pharmaceutical Sciences, Alfred E. Mann School of Pharmacy and Pharmaceutical Sciences, University of Southern California, Los Angeles, California 90089, United States*

Lei Zhang − *Department of Pharmacology and Pharmaceutical Sciences, Alfred E. Mann School of Pharmacy and Pharmaceutical Sciences, University of Southern California, Los Angeles, California 90089, United States*

Stan G. Louie − *Titus Family Department of Clinical Pharmacy, Alfred E. Mann School of Pharmacy and Pharmaceutical Sciences, University of Southern California, Los Angeles, California 90089, United States*

Vadim Cherezov − *Bridge Institute and Department of Chemistry, Dornsife College of Letters, Arts and Sciences, University of Southern California, Los Angeles, California 90089, United States;* orcid.org/0000-0002-5265-3914

Complete contact information is available at: https://pubs.acs.org/10.1021/jacsau.4c00695

Author Contributions

○G.K. and X.-N.Z. contributed equally to this work. G.K., X.-N.Z., and Y.Z. designed the research. G.K., X.-N.Z., F.N., B.B.K., Z.L., Z.D., Z.Z., and L.Z. performed the research. S.G.L. and V.C. provided the resources and critical insights. G.K., X.-N.Z., F.N., B.B.K., Z.L., V.C., and Y.Z. analyzed the data. G.K., X.-N.Z., and Y.Z. wrote the manuscript. CRediT: **Guoyun Kao** conceptualization, formal analysis, investigation, writing - original draft; **Xiao-Nan Zhang** conceptualization, formal analysis, investigation, writing - original draft; **Fariborz Nasertorabi** formal analysis, investigation; **Benjamin B. Katz** formal analysis, investigation; **Zeyang Li** formal analysis, investigation; **Zhefu Dai** investigation; **Zeyu Zhang** investigation; **Lei Zhang** investigation; **Stan G. Louie** resources; **Vadim Cherezov** formal analysis, resources; **Yong Zhang** conceptualization, formal analysis, funding acquisition, writing - original draft, writing - review & editing.

Notes

The authors declare no competing financial interest.

■ ACKNOWLEDGMENTS

We would like to thank the staff at the Stanford Synchrotron Radiation Lightsource (SSRL) beamline 12-1 and the

Advanced Photon Source (APS) beamline 23-ID-B for their excellent support during data collections. G.K. acknowledges the financial support from the USC Taiwan Global Fellowship. This work was supported in part by the Sharon L. Cockrell Cancer Research Fund, National Institute of General Medical Sciences (NIGMS) of the National Institutes of Health (NIH) grant R35GM137901 (to Y.Z.), the National Institute of Biomedical Imaging and Bioengineering (NIBIB) of the NIH grant R01EB031830 (to Y.Z.), and the National Cancer Institute (NCI) of NIH grant R01CA276240 (to Y.Z.).

REFERENCES

(1) Dai, Z.; Zhang, X. N.; Nasertorabi, F.; Cheng, Q.; Pei, H.; Louie, S. G.; Stevens, R. C.; Zhang, Y. Facile chemoenzymatic synthesis of a novel stable mimic of NAD^+. *Chem. Sci.* **2018**, *9* (44), 8337−8342.
(2) Imai, S.; Guarente, L. NAD+ and sirtuins in aging and disease. *Trends Cell Biol.* **2014**, *24* (8), 464−471.
(3) Lam, A. T.; Zhang, X. N.; Courouble, V. V.; Strutzenberg, T. S.; Pei, H.; Stiles, B. L.; Louie, S. G.; Griffin, P. R.; Zhang, Y. A Bifunctional NAD(+) for Profiling Poly-ADP-Ribosylation-Dependent Interacting Proteins. *ACS Chem. Biol.* **2021**, *16* (2), 389−396.
(4) Lin, H. Nicotinamide adenine dinucleotide: beyond a redox coenzyme. *Org. Biomol. Chem.* **2007**, *5* (16), 2541−2554.
(5) Verdin, E. NAD(+) in aging, metabolism, and neurodegeneration. *Science* **2015**, *350* (6265), 1208−1213.
(6) Zhang, X. N.; Lam, A. T.; Cheng, Q.; Courouble, V. V.; Strutzenberg, T. S.; Li, J.; Wang, Y.; Pei, H.; Stiles, B. L.; Louie, S. G.; Griffin, P. R.; Zhang, Y. Discovery of an NAD(+) analogue with enhanced specificity for PARP1. *Chem. Sci.* **2022**, *13* (7), 1982−1991.
(7) Stephens, E. N.; Zhang, X. N.; Lam, A. T.; Li, J.; Pei, H.; Louie, S. G.; Wang, C. C. C.; Zhang, Y. A ribose-functionalized NAD(+) with versatile activity for ADP-ribosylation. *Chem. Commun.* **2023**, *59* (93), 13843−13846.
(8) Kane, A. E.; Sinclair, D. A. Sirtuins and NAD(+) in the Development and Treatment of Metabolic and Cardiovascular Diseases. *Circ. Res.* **2018**, *123* (7), 868−885.
(9) Tarrago, M. G.; Chini, C. C. S.; Kanamori, K. S.; Warner, G. M.; Caride, A.; de Oliveira, G. C.; Rud, M.; Samani, A.; Hein, K. Z.; Huang, R.; Jurk, D.; Cho, D. S.; Boslett, J. J.; Miller, J. D.; Zweier, J. L.; Passos, J. F.; Doles, J. D.; Becherer, D. J.; Chini, E. N. A Potent and Specific CD38 Inhibitor Ameliorates Age-Related Metabolic Dysfunction by Reversing Tissue NAD(+) Decline. *Cell Metabol.* **2018**, *27* (5), 1081−1095 e10.
(10) Katsyuba, E.; Romani, M.; Hofer, D.; Auwerx, J. NAD(+) homeostasis in health and disease. *Nat. Metab.* **2020**, *2* (1), 9−31.
(11) Zeidler, J. D.; Hogan, K. A.; Agorrody, G.; Peclat, T. R.; Kashyap, S.; Kanamori, K. S.; Gomez, L. S.; Mazdeh, D. Z.; Warner, G. M.; Thompson, K. L.; Chini, C. C. S.; Chini, E. N. The CD38 glycohydrolase and the NAD sink: implications for pathological conditions. *Am. J. Physiol. Cell Physiol.* **2022**, *322* (3), C521−C545.
(12) Frederick, D. W.; Loro, E.; Liu, L.; Davila, A., Jr.; Chellappa, K.; Silverman, I. M.; Quinn, W. J., 3rd; Gosai, S. J.; Tichy, E. D.; Davis, J. G.; Mourkioti, F.; Gregory, B. D.; Dellinger, R. W.; Redpath, P.; Migaud, M. E.; Nakamaru-Ogiso, E.; Rabinowitz, J. D.; Khurana, T. S.; Baur, J. A. Loss of NAD Homeostasis Leads to Progressive and Reversible Degeneration of Skeletal Muscle. *Cell Metabol.* **2016**, *24* (2), 269−282.
(13) Camacho-Pereira, J.; Tarrago, M. G.; Chini, C. C. S.; Nin, V.; Escande, C.; Warner, G. M.; Puranik, A. S.; Schoon, R. A.; Reid, J. M.; Galina, A.; Chini, E. N. CD38 Dictates Age-Related NAD Decline and Mitochondrial Dysfunction through an SIRT3-Dependent Mechanism. *Cell Metabol.* **2016**, *23* (6), 1127−1139.
(14) Gomes, A. P.; Price, N. L.; Ling, A. J.; Moslehi, J. J.; Montgomery, M. K.; Rajman, L.; White, J. P.; Teodoro, J. S.; Wrann, C. D.; Hubbard, B. P.; Mercken, E. M.; Palmeira, C. M.; de Cabo, R.; Rolo, A. P.; Turner, N.; Bell, E. L.; Sinclair, D. A. Declining NAD(+) induces a pseudohypoxic state disrupting nuclear-mitochondrial communication during aging. *Cell* **2013**, *155* (7), 1624−1638.
(15) Bieganowski, P.; Brenner, C. Discoveries of nicotinamide riboside as a nutrient and conserved NRK genes establish a Preiss-Handler independent route to NAD+ in fungi and humans. *Cell* **2004**, *117* (4), 495−502.
(16) Tan, B.; Dong, S. C.; Shepard, R. L.; Kays, L.; Roth, K. D.; Geeganage, S.; Kuo, M. S.; Zhao, G. S. Inhibition of Nicotinamide Phosphoribosyltransferase (NAMPT), an Enzyme Essential for NAD(+) Biosynthesis, Leads to Altered Carbohydrate Metabolism in Cancer Cells. *J. Biol. Chem.* **2015**, *290* (25), 15812−15824.
(17) Canto, C.; Menzies, K. J.; Auwerx, J. NAD(+) Metabolism and the Control of Energy Homeostasis: A Balancing Act between Mitochondria and the Nucleus. *Cell Metabol.* **2015**, *22* (1), 31−53.
(18) Ghosh, S.; George, S.; Roy, U.; Ramachandran, D.; Kolthur-Seetharam, U. NAD: a master regulator of transcription. *Biochim. Biophys. Acta* **2010**, *1799* (10−12), 681−693.
(19) Zhang, T.; Kraus, W. L. SIRT1-dependent regulation of chromatin and transcription: linking NAD(+) metabolism and signaling to the control of cellular functions. *Biochim. Biophys. Acta* **2010**, *1804* (8), 1666−1675.
(20) Griffiths, H. B. S.; Williams, C.; King, S. J.; Allison, S. J. Nicotinamide adenine dinucleotide (NAD+): essential redox metabolite, co-substrate and an anti-cancer and anti-ageing therapeutic target. *Biochem. Soc. Trans.* **2020**, *48* (3), 733−744.
(21) Zhang, X.-N.; Cheng, Q.; Chen, J.; Lam, A. T.; Lu, Y.; Dai, Z.; Pei, H.; Evdokimov, N. M.; Louie, S. G.; Zhang, Y. A ribose-functionalized NAD+ with unexpected high activity and selectivity for protein poly-ADP-ribosylation. *Nat. Commun.* **2019**, *10* (1), 4196.
(22) Dai, Z.; Zhang, X.-N.; Cheng, Q.; Fei, F.; Hou, T.; Li, J.; Abdolvahabi, A.; Watanabe, J.; Pei, H.; Smbatyan, G.; Xie, J.; Lenz, H.-J.; Louie, S. G.; Zhang, Y. Site-specific antibody-drug conjugates with variable drug-to-antibody-ratios for AML therapy. *J. Controlled Release* **2021**, *336*, 433−442.
(23) Shi, X.; Zhang, X. N.; Chen, J.; Cheng, Q.; Pei, H.; Louie, S. G.; Zhang, Y. A poly-ADP-ribose polymer-based antibody-drug conjugate. *Chem. Sci.* **2020**, *11* (34), 9303−9308.
(24) Abdellatif, M.; Sedej, S.; Kroemer, G. NAD(+) Metabolism in Cardiac Health, Aging, and Disease. *Circulation* **2021**, *144* (22), 1795−1817.
(25) Yaku, K.; Okabe, K.; Nakagawa, T. NAD metabolism: Implications in aging and longevity. *Ageing Res. Rev.* **2018**, *47*, 1−17.
(26) Bresque, M.; Esteve, D.; Pehar, M.; Vargas, M. R. Nicotinamide Adenine Dinucleotide (NAD(+))-Dependent Signaling in Neurological Disorders. *Antioxid. Redox Signaling* **2023**, *39* (16−18), 1150−1166.
(27) Lee, H. C. Physiological functions of cyclic ADP-ribose and NAADP as calcium messengers. *Annu. Rev. Pharmacol. Toxicol.* **2001**, *41*, 317−345.
(28) Jiang, H.; Congleton, J.; Liu, Q.; Merchant, P.; Malavasi, F.; Lee, H. C.; Hao, Q.; Yen, A.; Lin, H. Mechanism-based small molecule probes for labeling CD38 on live cells. *J. Am. Chem. Soc.* **2009**, *131* (5), 1658−1659.
(29) Shrimp, J. H.; Hu, J.; Dong, M.; Wang, B. S.; MacDonald, R.; Jiang, H.; Hao, Q.; Yen, A.; Lin, H. Revealing CD38 cellular localization using a cell permeable, mechanism-based fluorescent small-molecule probe. *J. Am. Chem. Soc.* **2014**, *136* (15), 5656−5663.
(30) Lange, I.; Yamamoto, S.; Partida-Sanchez, S.; Mori, Y.; Fleig, A.; Penner, R. TRPM2 Functions as a Lysosomal Ca^{2+} -Release Channel in β Cells. *Sci. Signal.* **2009**, *2* (71), ra23.
(31) Liu, Q.; Kriksunov, I. A.; Graeff, R.; Lee, H. C.; Hao, Q. Structural basis for formation and hydrolysis of the calcium messenger cyclic ADP-ribose by human CD38. *J. Biol. Chem.* **2007**, *282* (8), 5853−5861.
(32) Lee, H. C.; Zhao, Y. J. Resolving the topological enigma in Ca(2+) signaling by cyclic ADP-ribose and NAADP. *J. Biol. Chem.* **2019**, *294* (52), 19831−19843.
(33) Zhang, X. N.; Dai, Z.; Cheng, Q.; Zhang, Y. Chemoenzymatic Preparation of 4′-Thioribose NAD^+. *Curr. Protoc. Nucleic Acid Chem.* **2019**, *77* (1), No. e83.

https://doi.org/10.1021/jacsau.4c00695
JACS Au 2024, 4, 4345−4360

(34) Liu, Q.; Kriksunov, I. A.; Moreau, C.; Graeff, R.; Potter, B. V.; Lee, H. C.; Hao, Q. Catalysis-associated conformational changes revealed by human CD38 complexed with a non-hydrolyzable substrate analog. *J. Biol. Chem.* **2007**, *282* (34), 24825−24832.
(35) Liu, Q.; Kriksunov, I. A.; Graeff, R.; Munshi, C.; Lee, H. C.; Hao, Q. Crystal structure of human CD38 extracellular domain. *Structure* **2005**, *13* (9), 1331−1339.
(36) Lee, H. C.; Zhao, Y. J. The type III calcium signaling mechanism of CD38. *Messenger* **2014**, *3* (1), 59−64.
(37) Liu, J.; Zhao, Y. J.; Li, W. H.; Hou, Y. N.; Li, T.; Zhao, Z. Y.; Fang, C.; Li, S. L.; Lee, H. C. Cytosolic interaction of type III human CD38 with CIB1 modulates cellular cyclic ADP-ribose levels. *Proc. Natl. Acad. Sci. U.S.A.* **2017**, *114* (31), 8283−8288.
(38) Wu, Y.; Zhang, J.; Fang, L.; Lee, H. C.; Zhao, Y. J. A cytosolic chaperone complex controls folding and degradation of type III CD38. *J. Biol. Chem.* **2019**, *294* (11), 4247−4258.
(39) Zhao, Y. J.; Lam, C. M.; Lee, H. C. The membrane-bound enzyme CD38 exists in two opposing orientations. *Sci. Signal.* **2012**, *5* (241), ra67.
(40) Peclat, T. R.; Thompson, K. L.; Warner, G. M.; Chini, C. C. S.; Tarrago, M. G.; Mazdeh, D. Z.; Zhang, C.; Zavala-Solorio, J.; Kolumam, G.; Liang Wong, Y.; Cohen, R. L.; Chini, E. N. CD38 inhibitor 78c increases mice lifespan and healthspan in a model of chronological aging. *Aging Cell* **2022**, *21* (4), No. e13589.
(41) de Zelicourt, A.; Fayssoil, A.; Dakouane-Giudicelli, M.; De Jesus, I.; Karoui, A.; Zarrouki, F.; Lefebvre, F.; Mansart, A.; Launay, J. M.; Piquereau, J.; Tarrago, M. G.; Bonay, M.; Forand, A.; Moog, S.; Pietri-Rouxel, F.; Brisebard, E.; Chini, C. C. S.; Kashyap, S.; Fogarty, M. J.; Sieck, G. C.; Mericskay, M.; Chini, E. N.; Gomez, A. M.; Cancela, J. M.; de la Porte, S. CD38-NADase is a new major contributor to Duchenne muscular dystrophic phenotype. *EMBO Mol. Med.* **2022**, *14* (5), No. e12860.
(42) Shi, B.; Wang, W.; Korman, B.; Kai, L.; Wang, Q.; Wei, J.; Bale, S.; Marangoni, R. G.; Bhattacharyya, S.; Miller, S.; Xu, D.; Akbarpour, M.; Cheresh, P.; Proccissi, D.; Gursel, D.; Espindola-Netto, J. M.; Chini, C. C. S.; de Oliveira, G. C.; Gudjonsson, J. E.; Chini, E. N.; Varga, J. Targeting CD38-dependent NAD(+) metabolism to mitigate multiple organ fibrosis. *iScience* **2021**, *24* (1), 101902.
(43) Chini, C. C. S.; Peclat, T. R.; Warner, G. M.; Kashyap, S.; Espindola-Netto, J. M.; de Oliveira, G. C.; Gomez, L. S.; Hogan, K. A.; Tarrago, M. G.; Puranik, A. S.; Agorrody, G.; Thompson, K. L.; Dang, K.; Clarke, S.; Childs, B. G.; Kanamori, K. S.; Witte, M. A.; Vidal, P.; Kirkland, A. L.; De Cecco, M.; Chellappa, K.; McReynolds, M. R.; Jankowski, C.; Tchkonia, T.; Kirkland, J. L.; Sedivy, J. M.; van Deursen, J. M.; Baker, D. J.; van Schooten, W.; Rabinowitz, J. D.; Baur, J. A.; Chini, E. N. CD38 ecto-enzyme in immune cells is induced during aging and regulates NAD(+) and NMN levels. *Nat. Metab.* **2020**, *2* (11), 1284−1304.
(44) Wang, L. F.; Huang, C. C.; Xiao, Y. F.; Guan, X. H.; Wang, X. N.; Cao, Q.; Liu, Y.; Huang, X.; Deng, L. B.; Deng, K. Y.; Xin, H. B. CD38 Deficiency Protects Heart from High Fat Diet-Induced Oxidative Stress Via Activating Sirt3/FOXO3 Pathway. *Cell. Physiol. Biochem.* **2018**, *48* (6), 2350−2363.
(45) Li, Y.; Liu, Y.; Zhang, Y.; Wu, Y.; Xing, Z.; Wang, J.; Fan, G. H. Discovery of a First-in-Class CD38 Inhibitor for the Treatment of Mitochondrial Myopathy. *J. Med. Chem.* **2023**, *66* (18), 12762−12775.
(46) Xie, L.; Wen, K.; Li, Q.; Huang, C. C.; Zhao, J. L.; Zhao, Q. H.; Xiao, Y. F.; Guan, X. H.; Qian, Y. S.; Gan, L.; Wang, L. F.; Deng, K. Y.; Xin, H. B. CD38 Deficiency Protects Mice from High Fat Diet-Induced Nonalcoholic Fatty Liver Disease through Activating NAD(+)/Sirtuins Signaling Pathways-Mediated Inhibition of Lipid Accumulation and Oxidative Stress in Hepatocytes. *Int. J. Biol. Sci.* **2021**, *17* (15), 4305−4315.
(47) Boslett, J.; Helal, M.; Chini, E.; Zweier, J. L. Genetic deletion of CD38 confers post-ischemic myocardial protection through preserved pyridine nucleotides. *J. Mol. Cell. Cardiol.* **2018**, *118*, 81−94.
(48) Lagu, B.; Wu, X.; Kulkarni, S.; Paul, R.; Becherer, J. D.; Olson, L.; Ravani, S.; Chatzianastasiou, A.; Papapetropoulos, A.; Andrzejewski, S. Orally Bioavailable Enzymatic Inhibitor of CD38, MK-0159, Protects against Ischemia/Reperfusion Injury in the Murine Heart. *J. Med. Chem.* **2022**, *65* (13), 9418−9446.
(49) Roboon, J.; Hattori, T.; Ishii, H.; Takarada-Iemata, M.; Nguyen, D. T.; Heer, C. D.; O'Meally, D.; Brenner, C.; Yamamoto, Y.; Okamoto, H.; Higashida, H.; Hori, O. Inhibition of CD38 and supplementation of nicotinamide riboside ameliorate lipopolysaccharide-induced microglial and astrocytic neuroinflammation by increasing NAD^+. *J. Neurochem.* **2021**, *158* (2), 311−327.
(50) Blacher, E.; Dadali, T.; Bespalko, A.; Haupenthal, V. J.; Grimm, M. O.; Hartmann, T.; Lund, F. E.; Stein, R.; Levy, A. Alzheimer's disease pathology is attenuated in a CD38-deficient mouse model. *Ann. Neurol.* **2015**, *78* (1), 88−103.
(51) Gasparrini, M.; Sorci, L.; Raffaelli, N. Enzymology of extracellular NAD metabolism. *Cell. Mol. Life Sci.* **2021**, *78* (7), 3317−3331.
(52) Yaku, K.; Palikhe, S.; Izumi, H.; Yoshida, T.; Hikosaka, K.; Hayat, F.; Karim, M.; Iqbal, T.; Nitta, Y.; Sato, A.; Migaud, M. E.; Ishihara, K.; Mori, H.; Nakagawa, T. BST1 regulates nicotinamide riboside metabolism via its glycohydrolase and base-exchange activities. *Nat. Commun.* **2021**, *12* (1), 6767.
(53) Sauve, A. A.; Deng, H. T.; Angeletti, R. H.; Schramm, V. L. A covalent intermediate in CD38 is responsible for ADP-ribosylation and cyclization reactions. *J. Am. Chem. Soc.* **2000**, *122* (33), 7855−7859.
(54) Dai, Z.; Zhang, X. N.; Nasertorabi, F.; Cheng, Q.; Li, J.; Katz, B. B.; Smbatyan, G.; Pei, H.; Louie, S. G.; Lenz, H. J.; Stevens, R. C.; Zhang, Y. Synthesis of site-specific antibody-drug conjugates by ADP-ribosyl cyclases. *Sci. Adv.* **2020**, *6* (23), No. eaba6752.
(55) Graeff, R. M.; Walseth, T. F.; Fryxell, K.; Branton, W. D.; Lee, H. C. Enzymatic synthesis and characterizations of cyclic GDP-ribose. A procedure for distinguishing enzymes with ADP-ribosyl cyclase activity. *J. Biol. Chem.* **1994**, *269* (48), 30260−30267.
(56) Wang, D.; Sennari, Y.; Shen, M.; Morita, K.; Kanazawa, T.; Yoshida, Y. ERK is involved in the differentiation and function of dimethyl sulfoxide-induced HL-60 neutrophil-like cells, which mimic inflammatory neutrophils. *Int. Immunopharmacol.* **2020**, *84*, 106510.
(57) Tasseff, R.; Jensen, H. A.; Congleton, J.; Dai, D.; Rogers, K. V.; Sagar, A.; Bunaciu, R. P.; Yen, A.; Varner, J. D. An Effective Model of the Retinoic Acid Induced HL-60 Differentiation Program. *Sci. Rep.* **2017**, *7* (1), 14327.
(58) Ratajczak, J.; Joffraud, M.; Trammell, S. A.; Ras, R.; Canela, N.; Boutant, M.; Kulkarni, S. S.; Rodrigues, M.; Redpath, P.; Migaud, M. E.; Auwerx, J.; Yanes, O.; Brenner, C.; Canto, C. NRK1 controls nicotinamide mononucleotide and nicotinamide riboside metabolism in mammalian cells. *Nat. Commun.* **2016**, *7*, 13103.
(59) Canto, C.; Houtkooper, R. H.; Pirinen, E.; Youn, D. Y.; Oosterveer, M. H.; Cen, Y.; Fernandez-Marcos, P. J.; Yamamoto, H.; Andreux, P. A.; Cettour-Rose, P.; Gademann, K.; Rinsch, C.; Schoonjans, K.; Sauve, A. A.; Auwerx, J. The NAD(+) precursor nicotinamide riboside enhances oxidative metabolism and protects against high-fat diet-induced obesity. *Cell Metabol.* **2012**, *15* (6), 838−847.
(60) Martens, C. R.; Denman, B. A.; Mazzo, M. R.; Armstrong, M. L.; Reisdorph, N.; McQueen, M. B.; Chonchol, M.; Seals, D. R. Chronic nicotinamide riboside supplementation is well-tolerated and elevates NAD(+) in healthy middle-aged and older adults. *Nat. Commun.* **2018**, *9* (1), 1286.
(61) Vannini, N.; Campos, V.; Girotra, M.; Trachsel, V.; Rojas-Sutterlin, S.; Tratwal, J.; Ragusa, S.; Stefanidis, E.; Ryu, D.; Rainer, P. Y.; Nikitin, G.; Giger, S.; Li, T. Y.; Semilietof, A.; Oggier, A.; Yersin, Y.; Tauzin, L.; Pirinen, E.; Cheng, W. C.; Ratajczak, J.; Canto, C.; Ehrbar, M.; Sizzano, F.; Petrova, T. V.; Vanhecke, D.; Zhang, L.; Romero, P.; Nahimana, A.; Cherix, S.; Duchosal, M. A.; Ho, P. C.; Deplancke, B.; Coukos, G.; Auwerx, J.; Lutolf, M. P.; Naveiras, O. The NAD-Booster Nicotinamide Riboside Potently Stimulates Hematopoiesis through Increased Mitochondrial Clearance. *Cell Stem Cell* **2019**, *24* (3), 405−418.e7.

https://doi.org/10.1021/jacsau.4c00695
JACS Au 2024, 4, 4345−4360

(62) Vreones, M.; Mustapic, M.; Moaddel, R.; Pucha, K. A.; Lovett, J.; Seals, D. R.; Kapogiannis, D.; Martens, C. R. Oral nicotinamide riboside raises NAD+ and lowers biomarkers of neurodegenerative pathology in plasma extracellular vesicles enriched for neuronal origin. *Aging Cell* **2023**, *22* (1), No. e13754.
(63) Tannous, C.; Ghali, R.; Karoui, A.; Habeichi, N. J.; Amin, G.; Booz, G. W.; Mericskay, M.; Refaat, M.; Zouein, F. A. Nicotinamide Riboside Supplementation Restores Myocardial Nicotinamide Adenine Dinucleotide Levels, Improves Survival, and Promotes Protective Environment Post Myocardial Infarction. *Cardiovasc. Drugs Ther.* **2023**, 1−12.
(64) Lv, J.; Liu, C. Y.; Guo, Y. F.; Feng, G. J.; Dong, H. SnCl2-Catalyzed Acetalation/Selective Benzoylation Sequence for the Synthesis of Orthogonally Protected Glycosyl Acceptors. *Eur. J. Org Chem.* **2022**, *2022* (33), No. e202101565.
(65) Kim, H. S.; Hariri, K.; Zhang, X. N.; Chen, L. C.; Katz, B. B.; Pei, H.; Louie, S. G.; Zhang, Y. Synthesis of site-specific Fab-drug conjugates using ADP-ribosyl cyclases. *Protein Sci.* **2024**, *33* (4), No. e4924.
(66) Evans, P. Scaling and assessment of data quality. *Acta Crystallogr., Sect. D: Biol. Crystallogr.* **2006**, *62*, 72−82.
(67) Kabsch, W. XDS. *Acta Crystallogr., Sect. D: Biol. Crystallogr.* **2010**, *66* (2), 125−132.
(68) Winn, M. D.; Ballard, C. C.; Cowtan, K. D.; Dodson, E. J.; Emsley, P.; Evans, P. R.; Keegan, R. M.; Krissinel, E. B.; Leslie, A. G. W.; McCoy, A.; McNicholas, S. J.; Murshudov, G. N.; Pannu, N. S.; Potterton, E. A.; Powell, H. R.; Read, R. J.; Vagin, A.; Wilson, K. S. Overview of the CCP4 suite and current developments. *Acta Crystallogr., Sect. D: Biol. Crystallogr.* **2011**, *67*, 235−242.
(69) Mccoy, A. J.; Grosse-Kunstleve, R. W.; Adams, P. D.; Winn, M. D.; Storoni, L. C.; Read, R. J. Phaser crystallographic software. *J. Appl. Crystallogr.* **2007**, *40*, 658−674.
(70) Langer, G.; Cohen, S. X.; Lamzin, V. S.; Perrakis, A. Automated macromolecular model building for X-ray crystallography using ARP/wARP version 7. *Nat. Protoc.* **2008**, *3* (7), 1171−1179.
(71) Emsley, P.; Cowtan, K. Coot: model-building tools for molecular graphics. *Acta Crystallogr., Sect. D: Biol. Crystallogr.* **2004**, *60*, 2126−2132.
(72) Murshudov, G. N.; Vagin, A. A.; Dodson, E. J. Refinement of macromolecular structures by the maximum-likelihood method. *Acta Crystallogr., Sect. D: Biol. Crystallogr.* **1997**, *53*, 240−255.
(73) Liebschner, D.; Afonine, P. V.; Baker, M. L.; Bunkóczi, G.; Chen, V. B.; Croll, T. I.; Hintze, B.; Hung, L.-W.; Jain, S.; McCoy, A. J.; et al. Macromolecular structure determination using X-rays, neutrons and electrons: recent developments in Phenix. *Acta Crystallogr., Sect. D: Struct. Biol.* **2019**, *75* (10), 861−877.

https://doi.org/10.1021/jacsau.4c00695
JACS Au 2024, 4, 4345−4360